REPORT DOCUMENTATION PAGE

Form Approved
OMB No. 0704-0188

1. AGENCY USE ONLY (Leave blank)	2. REPORT DATE	3. REPORT TYPE AND DATES COVERED
	June, 1996	Final Report, July 1,1993-Dec.31, 1995

4. TITLE AND SUBTITLE
Uppermost Mantle Structure in Southern Eurasia from PN Tomography and Sn Attenuation

5. FUNDING NUMBERS
Contract
F49620-93-0429

6. AUTHOR(S)
Hearn, Thomas M. and Ni, James F.

7. PERFORMING ORGANIZATION NAME(S) AND ADDRESS(ES)
Dept. of Physics, 3D
New Mexico State University
Las Cruces, NM 88003

8. PERFORMING ORGANIZATION REPORT NUMBER

9. SPONSORING/MONITORING AGENCY NAME(S) AND ADDRESS(ES)
Air Force Office of Scientific Research
110 Duncan Ave., Suite B-115
Bolling AFB, Washington, DC 20332-0001

10. SPONSORING/MONITORING AGENCY REPORT NUMBER

11. SUPPLEMENTARY NOTES
Program Manager: Stanley K. Dickenson, 202-767-4964, AFOSR/NL

12a. DISTRIBUTION/AVAILABILITY STATEMENT
Unlimited

12b. DISTRIBUTION CODE

13. ABSTRACT *(Maximum 200 words)*

This project has investigated the seismic characteristics of southern Eurasia through Pn travel time tomography and the regional mapping of attenuation for high-frequency Sn and Lg waves. Pn tomography results indicate that much of the uppermost mantle beneath southern Eurasia has low P-wave velocity and a small amount of melt. Mapping of Sn propagation efficiency confirms that regions with low Pn velocity generally do not propagate Sn waves efficiently. This is especially true for the Turkish-Iranian Plateau and the northern Tibetan Plateau. In contrast to Sn waves, Lg waves propagate within the crust and are insensitive to mantle properties, but are affected by changes in crustal structure. Lg is weakened or completely absent when propagation paths obliquely cross major tectonic boundaries such as the Himalaya Mountains, the Tarim Basin, the Caucasus Mountains, or the oceanic crust of the Black and Caspian Seas. The high attenuation of Sn in many parts of southern Eurasia limits its use in regional nuclear monitoring; however, Lg can be observed provided data is available from stations sited within each geologic province.

14. SUBJECT TERMS	15. NUMBER OF PAGES
Seismology: Middle East Crust and Mantle Structure; Pn, Sn, Lg	58
	16. PRICE CODE

17. SECURITY CLASSIFICATION OF REPORT	18. SECURITY CLASSIFICATION OF THIS PAGE	19. SECURITY CLASSIFICATION OF ABSTRACT	20. LIMITATION OF ABSTRACT
Unclassified	Unclassified	Unclassified	UL

NSN 7540-01-280-5500

Standard Form 298 (Rev. 2-89)
Prescribed by ANSI Std. Z39-18
298-102

DISCLAIMER NOTICE

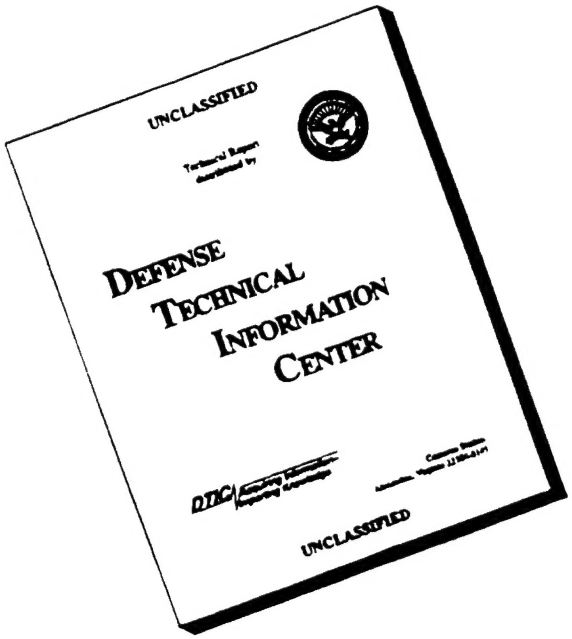

THIS DOCUMENT IS BEST QUALITY AVAILABLE. THE COPY FURNISHED TO DTIC CONTAINED A SIGNIFICANT NUMBER OF PAGES WHICH DO NOT REPRODUCE LEGIBLY.

Final Technical Report, June 1996

Uppermost Mantle Structure in Southern Eurasia from Pn Tomography and Sn Attenuation

Air Force Office of Scientific Research Contract No. F49620-93-1-0429
Contract Period: July 1, 1993 to December 31, 1995.
Principal Investigators: Thomas Hearn and James Ni.
New Mexico State University, Department of Physics, Las Cruces, NM, USA

Contents

List of Figures

Summary

This project has investigated the seismic characteristics of southern Eurasia through Pn travel time tomography and the regional mapping of attenuation for high-frequency Sn and Lg waves. Pn tomography results indicate that much of the uppermost mantle beneath southern Eurasia has low P-wave velocity and a small amount of melt. Mapping of Sn propagation efficiency confirms that regions with low Pn velocity generally do not propagate Sn waves efficiently. This is especially true for the Turkish-Iranian Plateau and the northern Tibetan Plateau. In contrast to Sn waves, Lg waves propagate within the crust and are insensitive to mantle properties, but are affected by changes in crustal structure. Lg is weakened or completely absent when propagation paths obliquely cross major tectonic boundaries such as the Himalaya Mountains, the Tarim Basin, the Caucasus Mountains, or the oceanic crust of the Black and Caspian Seas. The high attenuation of Sn in many parts of southern Eurasia limits its use in regional nuclear monitoring; however, Lg can be observed provided data is available from stations sited within each geologic province.

Research Accomplished

Introduction

Regional wave propagation studies have long been useful in problems associated with the proliferation of nuclear weapons. Regional studies serve a twofold purpose: (1) regional data can provide stable yield estimates for underground nuclear explosions, and (2) regional data can discriminate between explosions and earthquakes. For both of these goals, understanding the timing and strength of regional seismic phases is crucial. Regional seismic phases that are most useful in discrimination studies are the Pn, Sn, and Lg phases. Discriminants based on these types of regional data are generally not transportable and must be individually calibrated for a particular region. In this research, we study the characteristics of the Pn, Sn, and Lg seismic phases for southern Eurasia with an emphasis on the Middle East and Tibet. Regional variations of P-wave velocity and anisotropy in the uppermost mantle are found through the tomographic inversion of travel times. Sn and Lg propagation and attenuation are studied by a detailed examination of many thousands of raypaths for propagation efficiency.

The Pn phase corresponds to the raypaths that are critically reflected at the Moho discontinuity. It propagates as a true head wave at shorter distances and as a shallowly bottoming P-wave at farther distances. Thus, Pn travel times are sensitive to uppermost mantle P-wave velocities. Mantle velocities are, in turn, controlled by

mantle temperature and, to a lesser extent, composition. A global average for Pn velocity is 8.1 km/s (Christiansen and Mooney, 1995) with shields and platforms slightly faster (8.1-8.2 km/s), and continental orogens and rifts slower (7.9-8.0 km/s). In southern Eurasia, similar variations of Pn velocity are found. Chen and Molnar (1977) found low Pn velocities for paths beneath the Turkish Plateau (7.7 km/s) and faster velocities under Iran (8.0 km/s) with a possible dip in the Moho from north to south. Kadinsky-Cade et al. (1981) inferred faster Pn velocities (8.0-8.2 km/s) for the entire Turkish-Iranian Plateau. Southern Tibet has high Pn velocities (~8.2 km/s) while northern Tibet has lower velocities (~8.0 km/s) (McNamara et al., 1996). There is also evidence for substantial directional Pn velocity anisotropy which can be also found tomographically (Hearn, 1984; 1996).

Low Pn velocities (<7.8 km/s) suggest that small amounts (<2%) of partial melt may exist in the mantle beneath parts of the southern Eurasian convergent margin. If so, the Sn waves should be highly attenuated by the partial melt. Sn is the shear-wave analog of Pn and samples the shear-wave structure at the top of the mantle. Sn is the first arriving S-wave at regional distances (with group velocity of 4.7 km/s to 4.4 km/s) and is generally observed as an emergent arrival on transverse component seismograms. The ratio of Sn amplitudes to Pn amplitudes has been used as a measure of the shear-wave strength for a seismic event and can be used to differentiate an explosion from an earthquake. However, because Sn is a shear wave, it will not propagate if partial melt is present. Observations of the strength of Sn propagation have been used to infer physical properties of the mantle lid. Sn generally does not propagate across regions of high heat flow such as spreading centers, back-arcs and tectonically active continental regions (Molnar and Oliver, 1969), the Basin and Range Province (Beghoul and Barazangi, 1993) and the northern Tibetan Plateau (Ni and Barazangi, 1983; McNamara et al, 1995a). Kadinsky-Cade et al. (1981) indicated that much of the Turkish-Iranian Plateau does not propagate Sn.

Lg is also an important phase for seismic discrimination. It is a complex, short-period wavetrain with large amplitudes and group velocities in the range of 3.2 to 3.6 km/s. Lg has been modelled as a composite of higher-mode Love and Raleigh waves, or as a sequence of multiply reflected, post-critical S-waves trapped in the crustal wave guide (e.g. Bouchon, 1982; Kennett, 1986). Like Sn, it is also a shear wave whose amplitude can be used to determine the amount of shear energy of a seismic event. Lg is particularly useful in this regard since it averages seismic energy over the focal sphere and, thus, has an amplitude that is relatively insensitive to the orientation of the focal mechanism. An important observation is that Lg propagates efficiently in uniform continental shield crust, while it does not propagate across ocean basins (Press and Ewing, 1952). The amplitude of Lg is weakened by

attenuation (e.g. Ruzaikin, et al, 1977; Nuttli, 1980) and by variations in crustal structure along the path (e.g. Kennett, 1986). Kadinsky-Cade et al (1981) found such changes are produced by the oceanic crust of the Black Sea and the southern Caspian Sea and Ni and Barazangi (1983) found that Lg does not propagate across the edges of the Tibetan Plateau.

In this contract report, we summarize work done under this AFOSR contract and present a complete set of maps that illustrate the regional distribution of Pn velocity and Sn and Lg propagation characteristics. More detailed discussions of this work can be found in the publications that have resulted from the contract. The initial publication that led this contract was on the tomography of the Turkish Iranian Plateau (Hearn and Ni, 1994). Newer work on the anisotropic Pn tomography of southern Europe is currently being submitted for publication (Hearn and Wu, 1996). The tomography work has also been presented at national meetings (Hearn and Wu, 1995; Mele et al, 1995, Hearn and Ni, 1992a, b, c). The tomography study of the Turkish-Iranian Plateau was followed by a study of Sn and Lg propagation efficiency for the region. A manuscript is currently under review (Rodgers, Ni, and Hearn, 1996) and these results have also been presented at several meetings (Rodgers, Hearn and Ni, 1994a, b). Estimates of Lg attenuation for the Turkish-Iranian Plateau were also published (Wu, Ni, and Hearn, 1995a, b). Further mapping of Lg and Sn propagation in China have also been presented (Rapine et al., 1995; Ni et al., 1995) and are being prepared for submission (Rapine, Ni, and Hearn, 1996). This work on Chinese wave propagation began under this AFOSR contract and continues under a new grant administered by Phillips Geophysical Laboratory.

Pn tomography of the Middle East, southern Europe, Afghanistan, and Indochina

Techniques for seismic tomography using the Pn travel times are described in detail in Hearn and Ni (1994), and the extension to anisotropic tomography is reported in Hearn (1996). Basically, the Pn raypath can be divided into three segments: the crustal segment beneath the event, the crustal segment beneath the station, and the mantle segment of the raypath. Accordingly, the tomographic inversion of travel times solves for crustal time delays at each event, crustal time delays at each station, and lateral variations in mantle velocity and anisotropy. The event delays serve mostly to accommodate errors in event depth and origin time so little structural information can be gained from them. The crustal delays depend on both crustal thickness and crustal velocity structure and can be interpreted as such. Assuming a constant crustal velocity, one second delay corresponds to about 10 km of crustal thickness change; for a crust of constant thickness, one second of delay corresponds to a change in mean crustal velocity of about 1.6 km/s. The tomographically

estimated mantle velocity variations are mapped in plane view at the surface of the mantle and anisotropy variations can be similarly mapped. Pn velocities can be interpreted primarily in terms of mantle temperature variations, although composition is also important. Partial melt in mantle material begins to occur when mantle velocities drop by about 6% from normal values (Sato, et al., 1989). Thus, if the normal Pn velocity is 8.0-8.2 km/s, then velocities below about 7.7 km/s indicate the presence of partial melt. A large-scale map showing Pn velocity variations for southern Eurasia is in Figure 1. The regions covered by this map are studied in more detail with further tomography for the Turkish-Iranian Plateau, southern Europe, Afghanistan, and Indochina using travel time data from the ISC earthquake catalog (NEIC, 1990). These studies include error and resolution analyses that are described in publications.

The initial study was for the Turkish-Iranian Plateau (Figure 2) and results from Hearn and Ni (1994) are shown in Figures 3. On average, uppermost mantle P-wave velocity beneath the Turkish-Iranian Plateau is considerably slower than beneath continental shield regions. While normal Pn velocities (8.0-8.2 km/sec) were found under the Black Sea and Southern Caspian Sea, a region of anomalously low Pn velocities (<7.7 km/sec) exists beneath the high elevations of the Turkish-Iranian Plateau. This region coincides with a region of previously observed high Sn attenuation (Kadinsky-Cade, et al., 1981) and extensive Neogene volcanism. Teleseismic studies show that the low velocities extend at least 100 km into the upper mantle (Spakman, 1991). These structural features suggest that near solidus conditions exist within the uppermost mantle beneath the Turkish-Iranian Plateau and are probably the result of the oceanic subduction that occurred prior to continental collision. Such near solidus conditions could result from high temperature and the infiltration of water released from subducted lithosphere into the mantle above. The presence of a partially melted uppermost mantle weakens the lithosphere beneath the Turkish-Iranian Plateau, thus allowing it to become the locus of deformation in the Arabian-Russian collision zone. Station delays in the Lesser Caucasus region compare in magnitude to those found along the Aegean coast, indicating crustal thicknesses of 34 ± 9 km.

Stations in southern Europe have collected large numbers of Pn travel times. For this set of ISC derived data the regionally varying Pn velocity anisotropy was also estimated using the method of Hearn (1996). Results show that anisotropy is a significant portion of the tomographic inversion and that ignoring anisotropy can lead to false conclusions about the lateral variations of mantle velocity. For southern Europe, we resolved velocity and anisotropy variations in regions as small as 2 degrees squared. Both low Pn velocities and significant amounts of anisotropy are associated with the convergent margins of the Mediterranean Sea (Figures 4). Up to 4% (±0.37

km/s) anisotropy is found along the western Aegean arc and extends north into Albania. There, the fast axis of the anisotropy is oriented parallel to the arc. Anisotropy is also found beneath the Apennine Mountains and southern Italy. In those places, the fast axis of anisotropy is parallel to the Italian Peninsula and part of the Calabrian Arc. Arc parallel anisotropy could be due to either arc parallel flow or subduction generated compression. Arc parallel flow would cause anisotropy by aligning the olivine a-axes (fast axes) parallel to the flow direction. It would also raise the isotropic Pn velocity by about 0.15 km/s assuming ±0.3 km/s anisotropy. Arc compression would align the olivine b-axes (slow axes) parallel to the compression direction while lowering the isotropic Pn velocity by 0.15 km/s. Since most of these high anisotropy margins also have low (<8.0 km/s) Pn velocities, anisotropy by compression is a likely cause. These low velocities and high anisotropy are the signature of the mantle wedge created during subduction.

Pn tomography has also been applied to the Afghanistan region and to Indochina; however, limited data restricts the resolution to features of 4 degrees or more in width. Afghanistan and surrounding areas generally have high Pn velocities (~8.3 km/s), but low velocities (~7.9 km/s) exist beneath the southern flank of the Hindu-Kush Mountains (Figures 5). We believe that these low velocities are the signature of the altered mantle wedge formed during oceanic subduction. A low velocity mantle is also suggested for eastern Burma, but there the low velocities are related to continental rifting of the Pan-Xie Rift (Figures 6).

Regional Sn and Lg wave characteristics of the Middle East

The low Pn velocities beneath the Turkish-Iranian Plateau suggest the presence of partial melt in the uppermost mantle and that the observed high Sn attenuation (Kadinsky-Cade, et al., 1981) is also associated with this melt. To test this hypothesis, the study of Kadinsky-Cade was expanded using more recently available data from the now defunct Iranian Long Period Array (ILPA) (Akasheh et al., 1976) and Global Seismic Network (GSN) stations ABKT, ANTO, KEG, and KIV. ILPA data was obtained from Phillips Laboratory and GSN data from the Incorporated Research Institutions for Seismology - Data Management Center (IRIS-DMC). Event locations were taken from the Preliminary Determination of Epicenters (PDE) catalog produced by the International Seismological Centre (ISC). Besides measurements of Sn amplitude, amplitudes of the crustal phase Lg were also measured (Rodgers et al., 1996). Research on wave propagation characteristics was later extended to China using data collected by the Chinese Digital Seismic Network stations and temporary PASSCAL stations deployed in Pakistan and Tibet by New Mexico State University.

Figure 1: Pn velocities for southern Eurasia estimated from Pn tomography. Dark shades indicate higher velocities; light shades are slower velocities. Many of the low velocity regions are associated with small amounts of partial melt in the uppermost mantle.

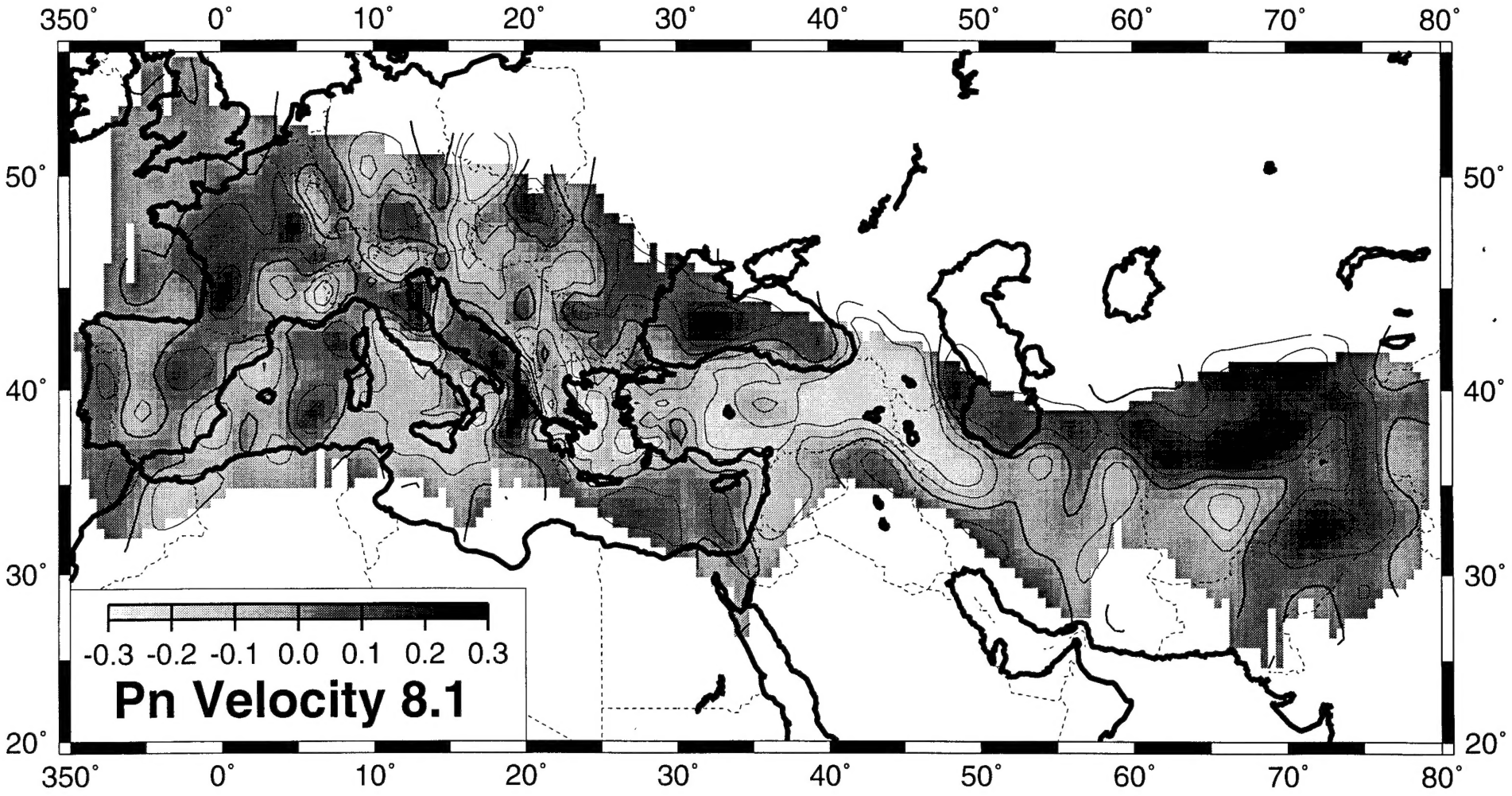

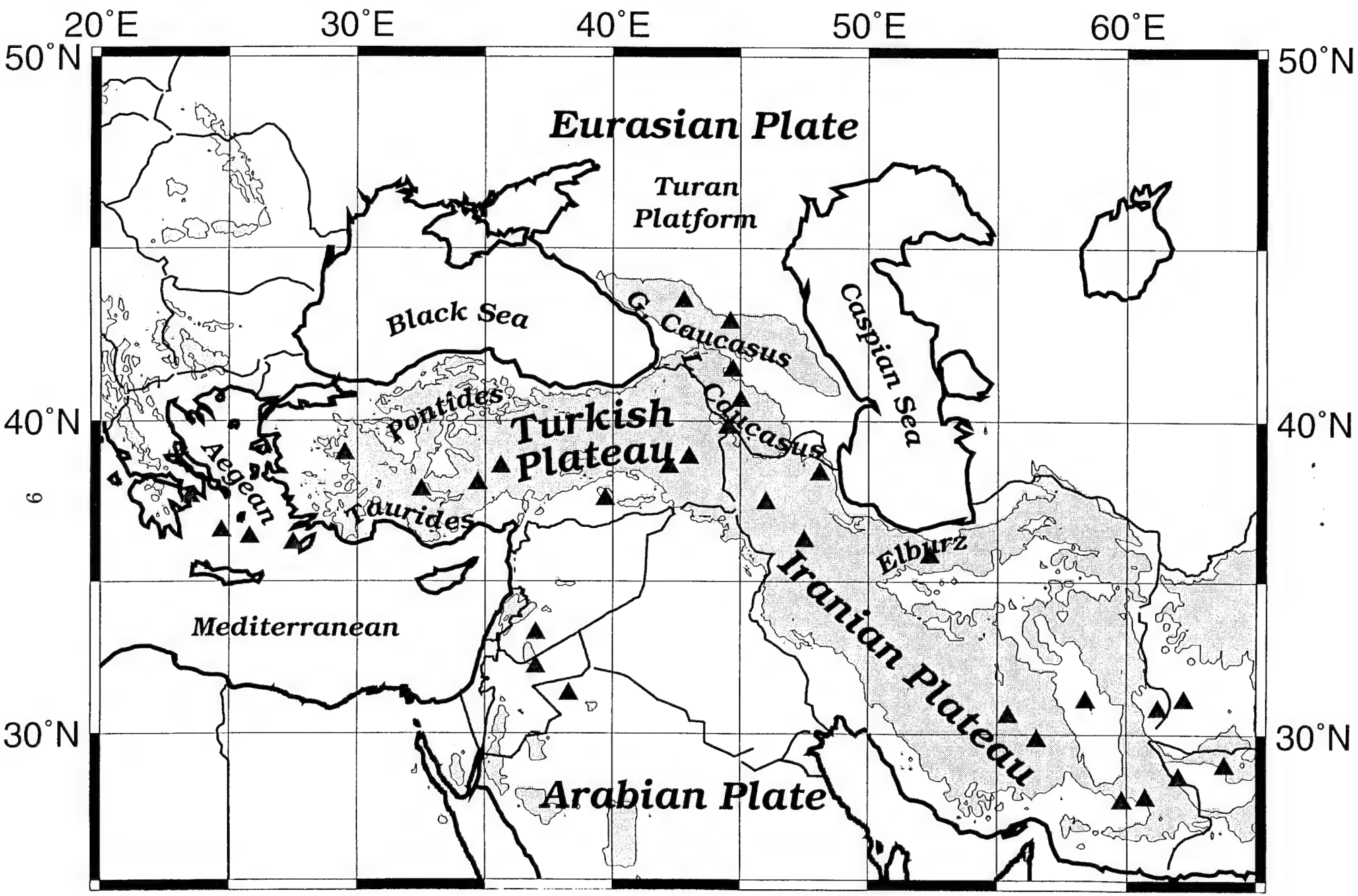

Figure 2: Location map for the Middle East. Shaded regions indicate regions over 1 km elevation.

Figure 3a: Raypaths used for Pn tomography of the Middle East.

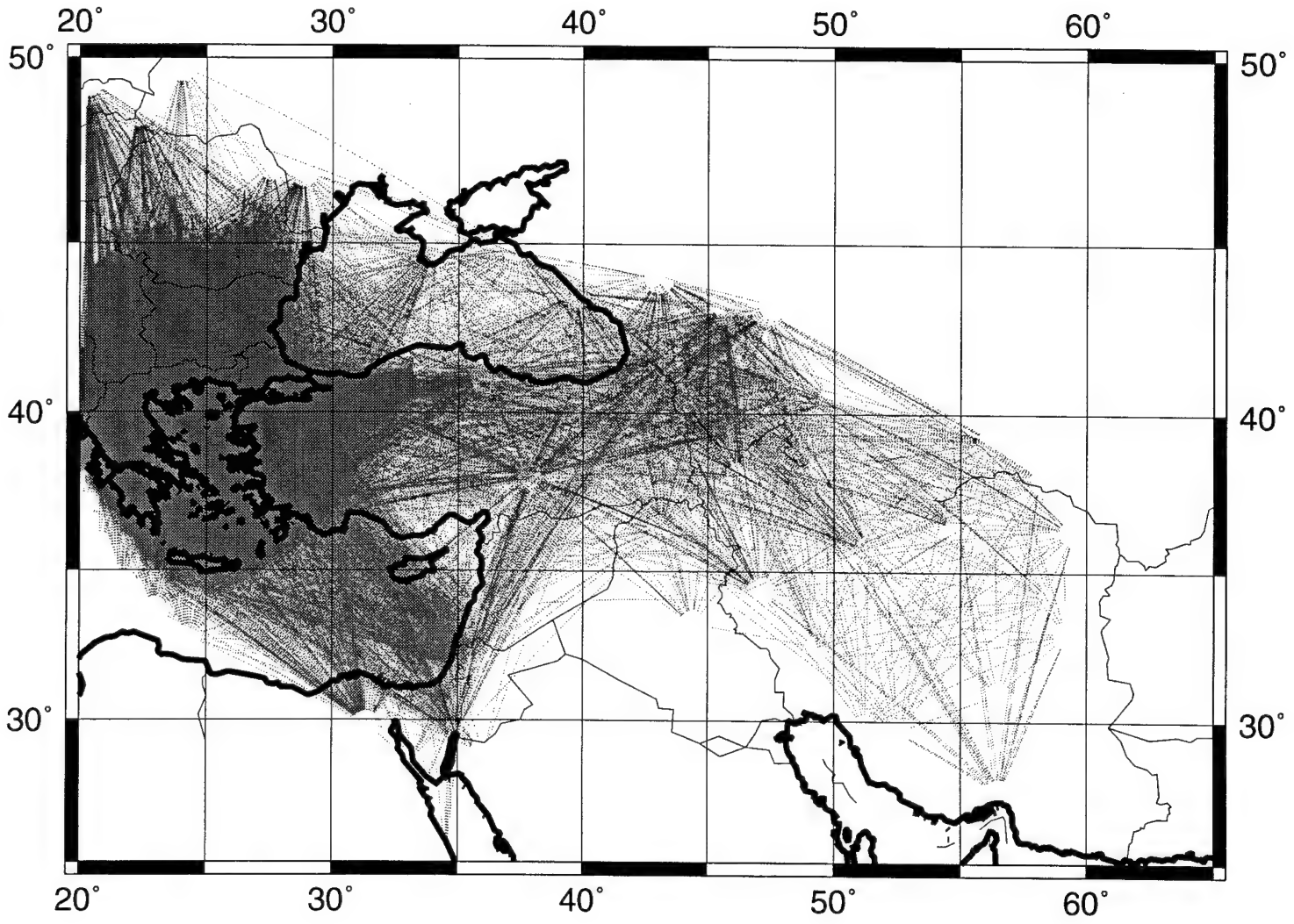

Figure 3b: Pn velocity for the Middle East relative to a mean Pn velocity of 8.0 km/s. The low velocities beneath the Turkish-Iranian Plateau suggest the presence of small amounts of partial melt in the uppermost mantle there. This inference is supported by the high Sn attenuation and the presence of regional volcanism on the Plateau.

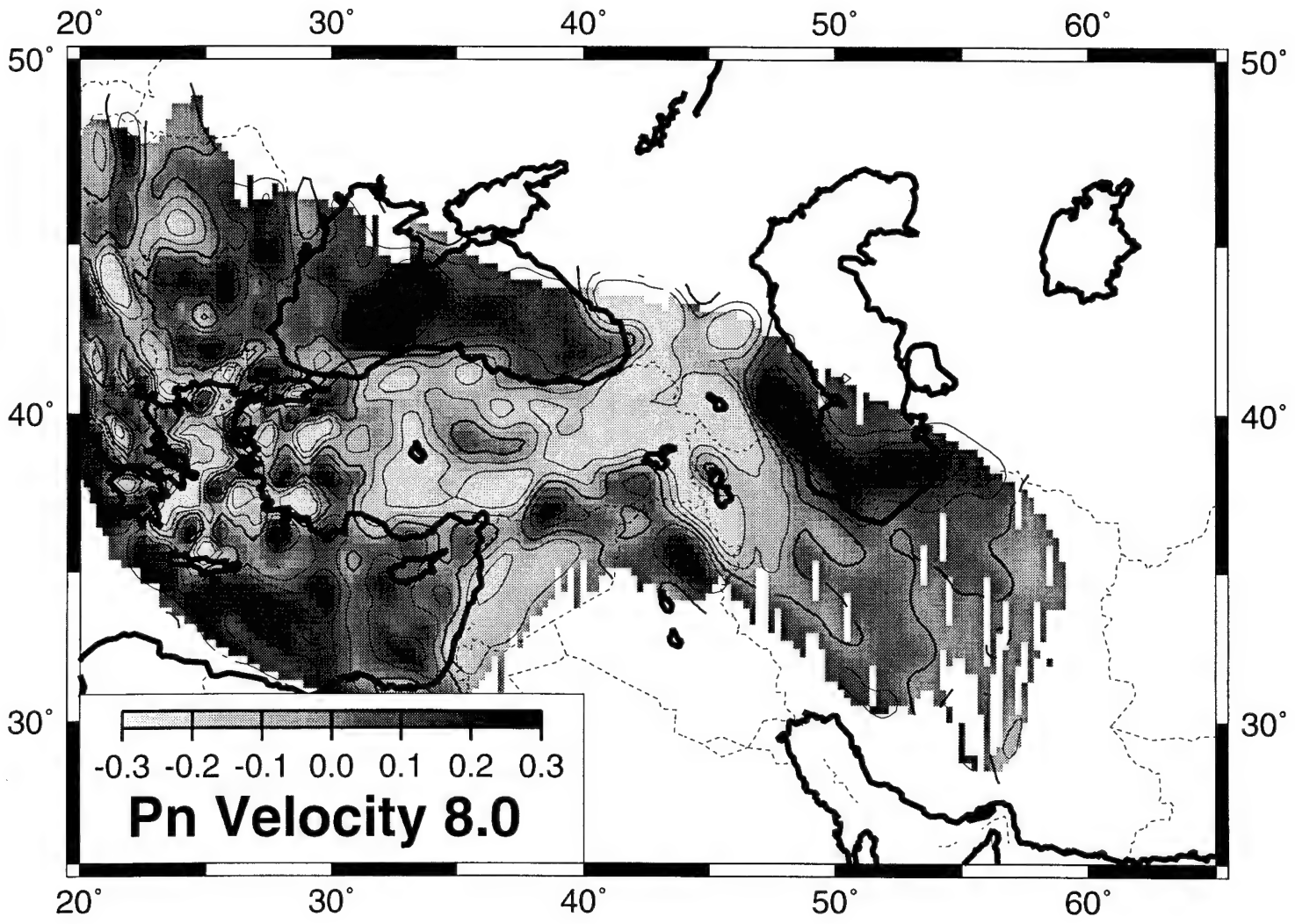

Figure 3c: Pn station delay times for the Middle East. Squares represent stations with early delays; circles represent those with late delays. A one second delay corresponds to about 10 km of crustal thickness change assuming constant crustal velocity; for a crust of constant thickness, one second of delay corresponds to a change in mean crustal velocity of about 1.6 km/s.

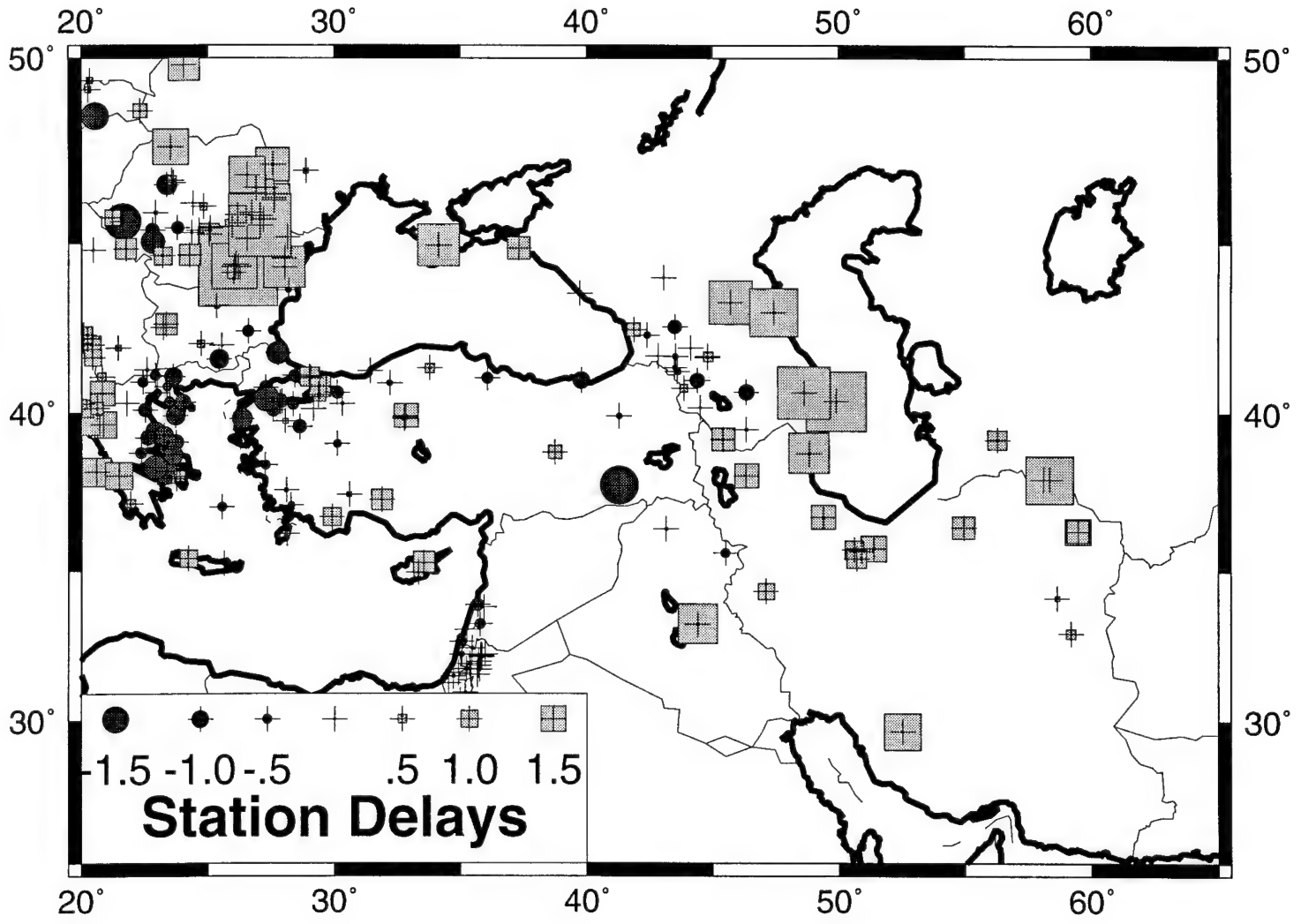

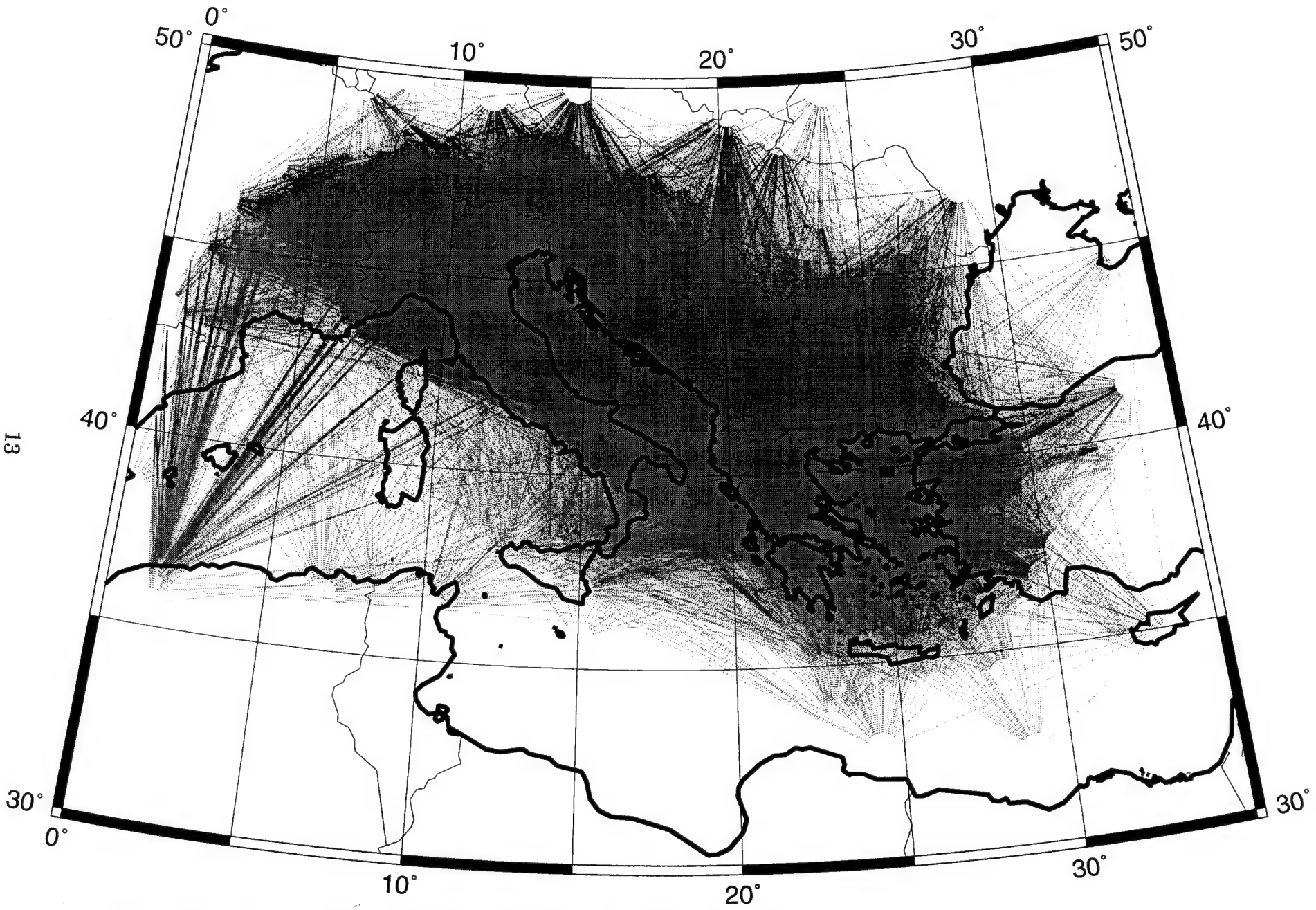

Figure 4a: Raypaths used for Pn tomography of southern Europe.

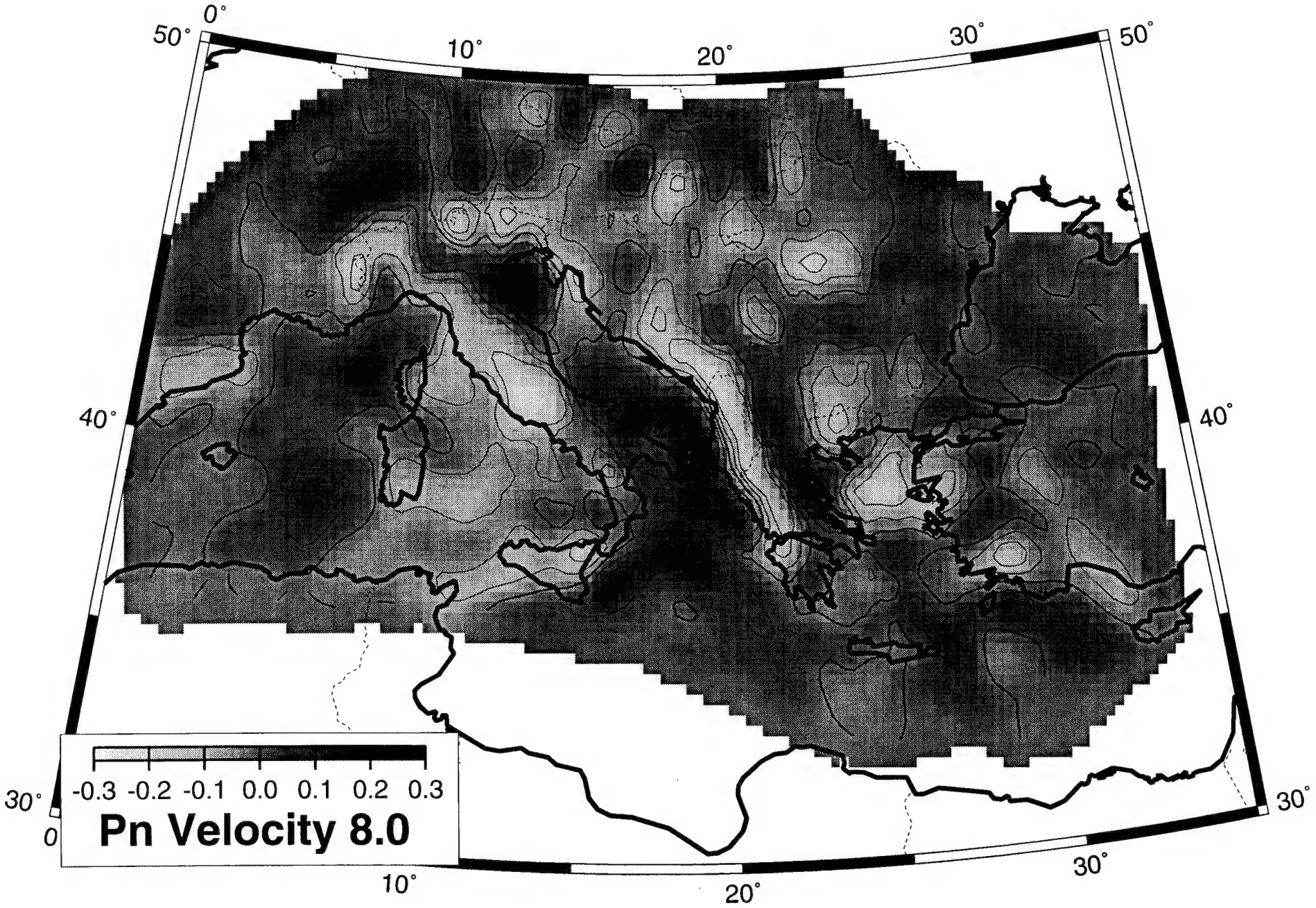

Figure 4b: Pn velocity for southern Europe relative to a mean Pn velocity of 8.0 km/s.

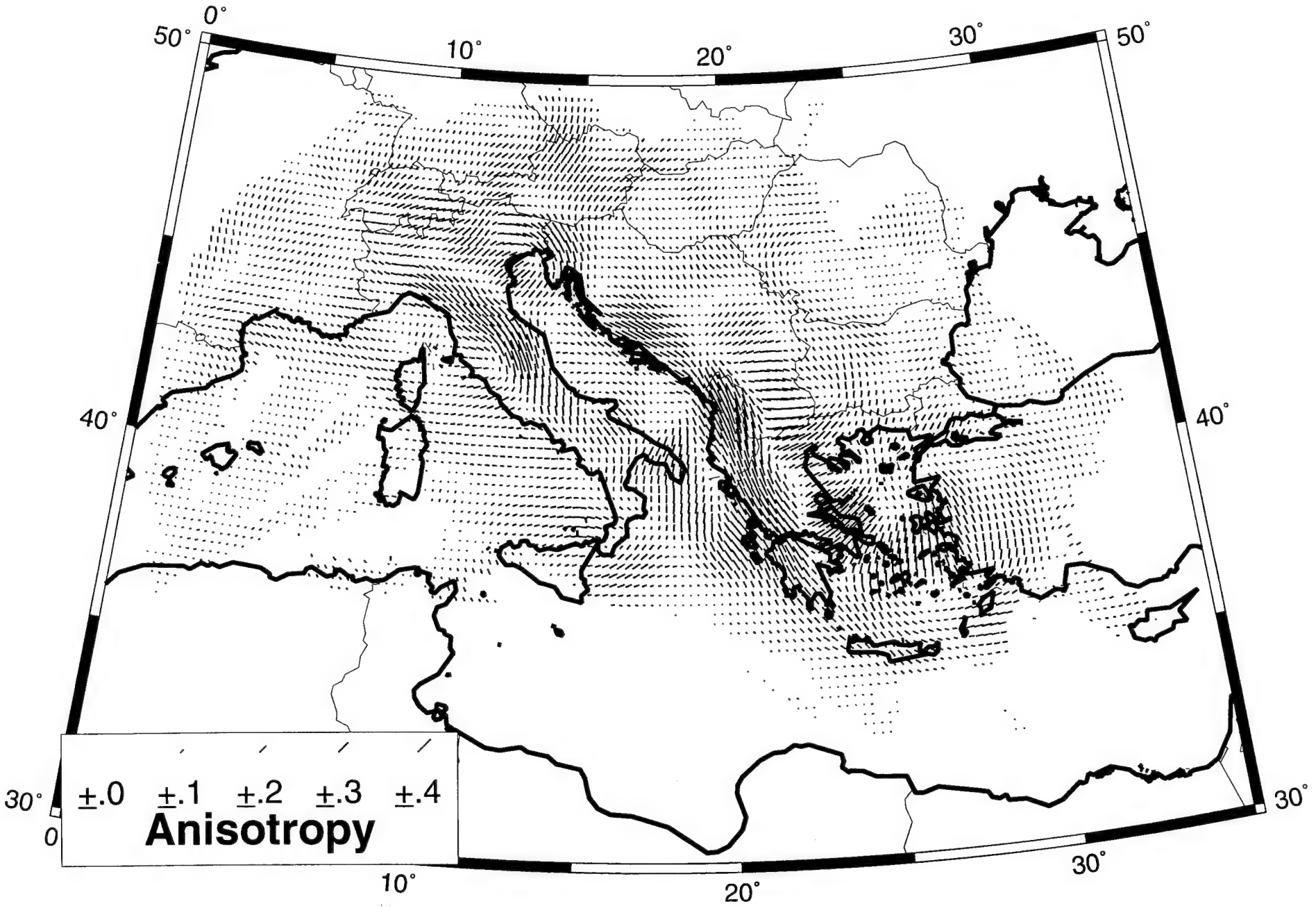

Figure 4c: Pn anisotropy for southern Europe. Each line segment is oriented in the direction of highest Pn velocity; line segment lengths are proportional to the amount of anisotropy.

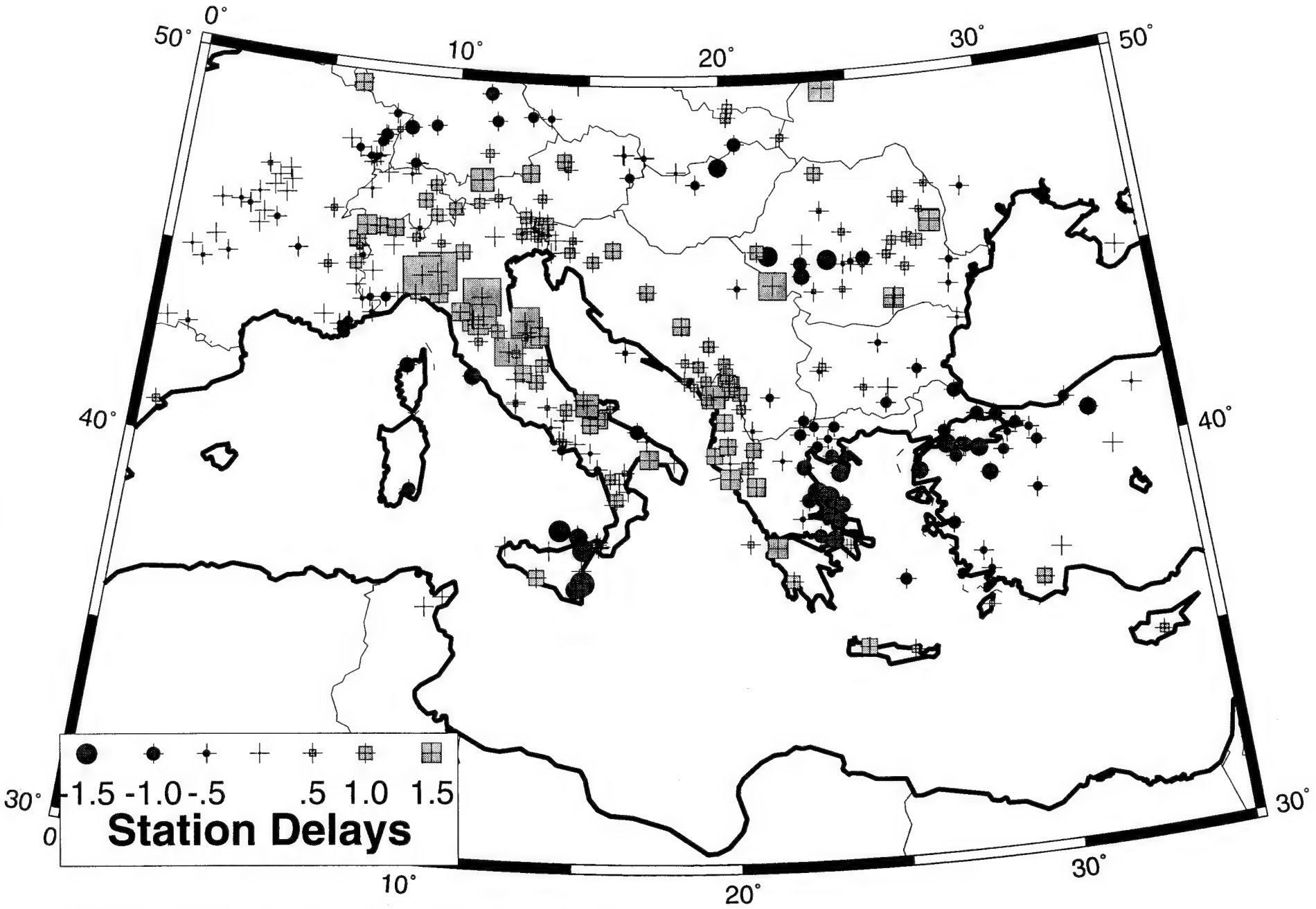

Figure 4d: Pn station delay times for southern Europe.

Figure 5a: Raypaths used for Pn tomography of Afghanistan.

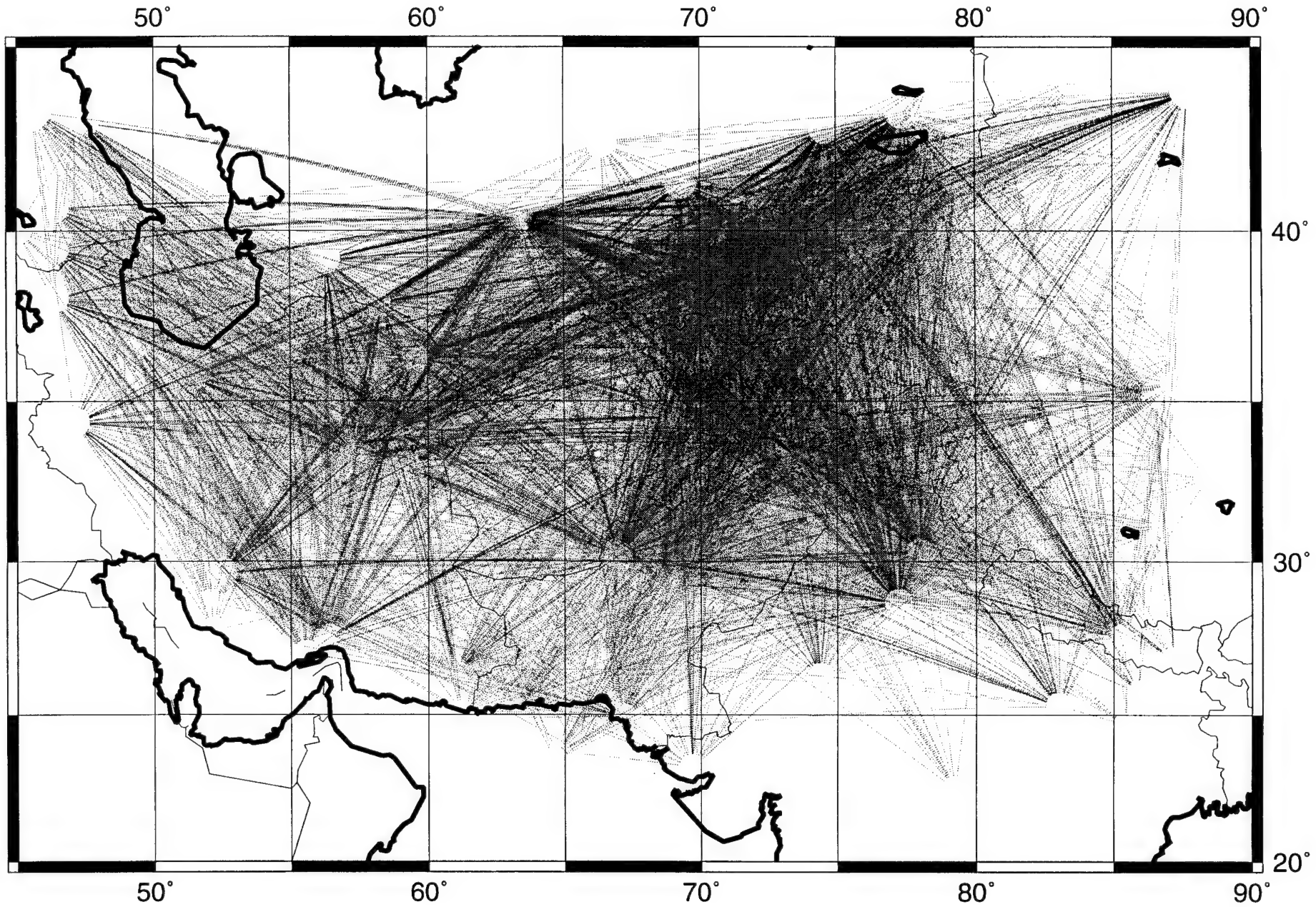

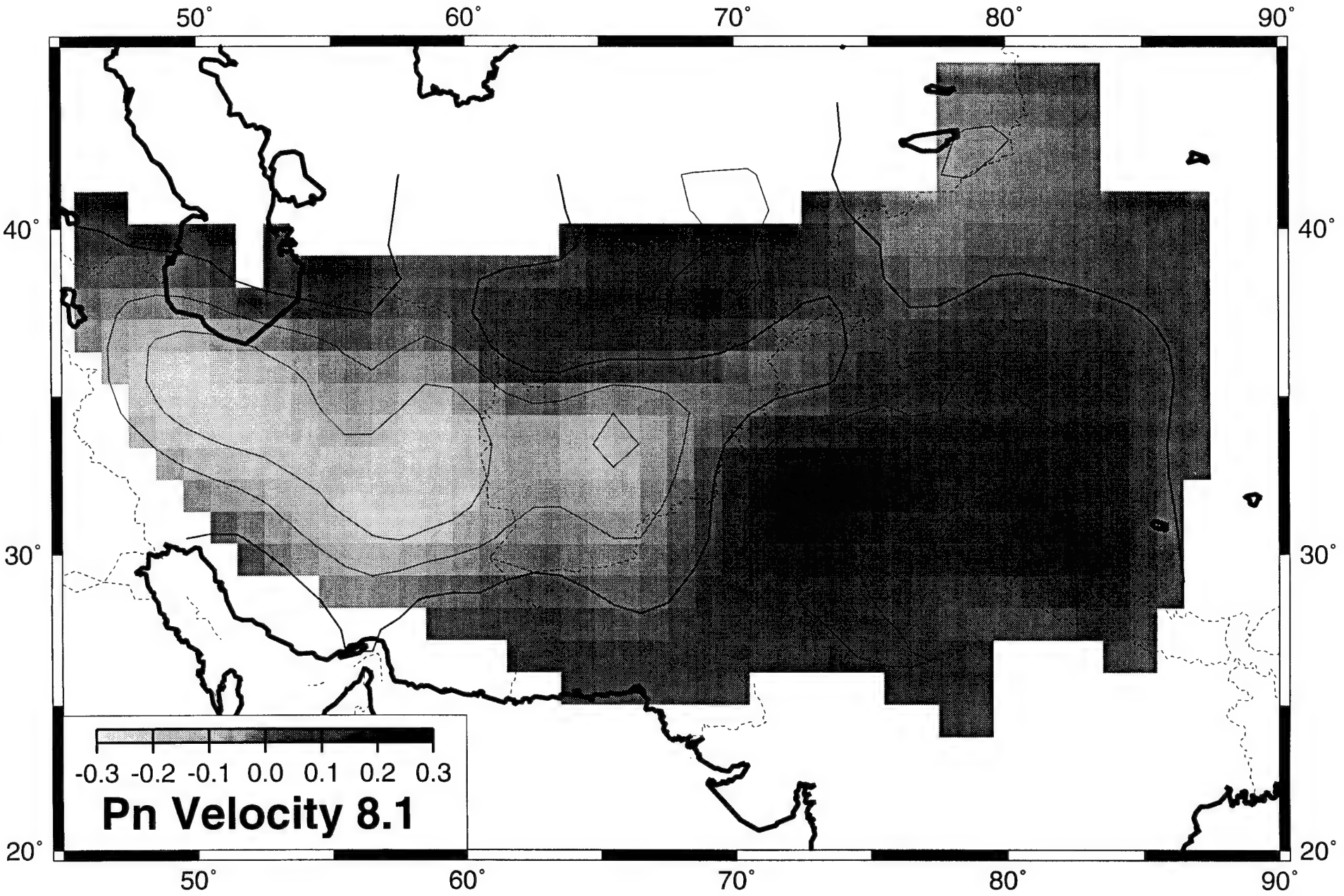

Figure 5b: Pn velocity for Afghanistan and surrounding regions relative to a mean velocity of 8.1 km/s.

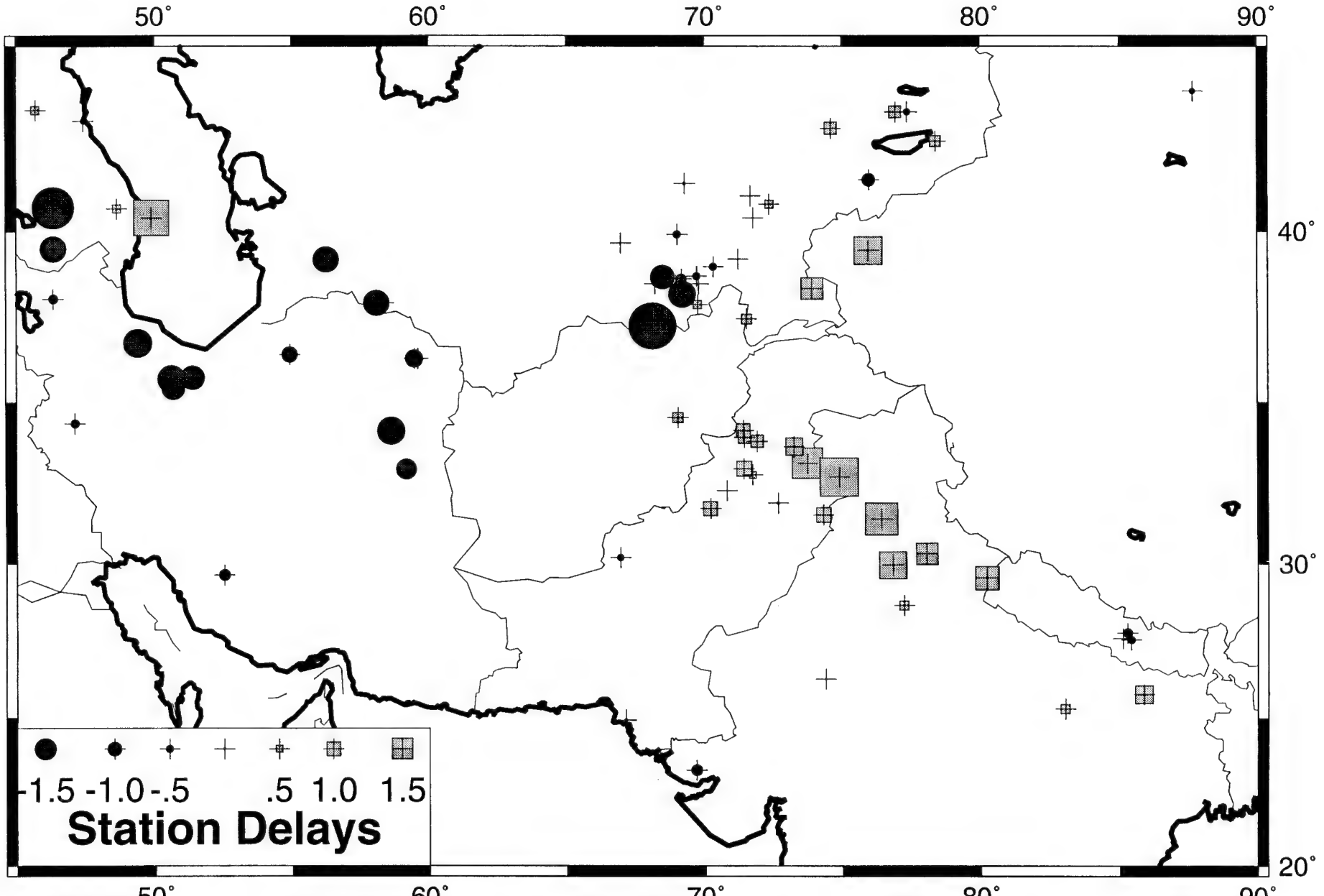

Figure 5c: Pn station delay times for Afghanistan. Due to the lack of data, the delays have high errors and are difficult to interpret.

Figure 6a: Raypaths used for Pn tomography of Indochina.

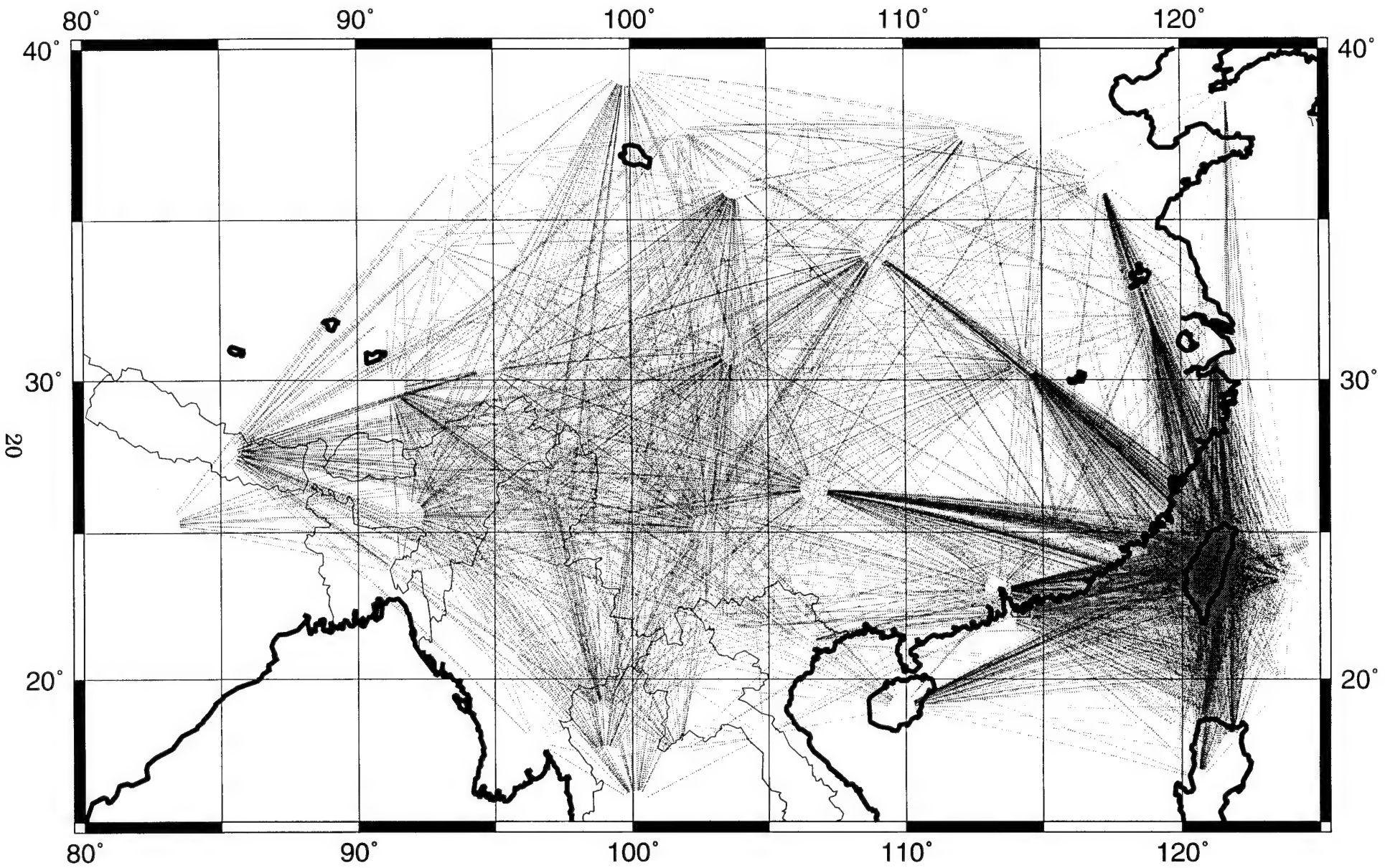

Figure 6b: Pn velocity for Indochina. Resolution is poor in this image; however, the low velocity region of eastern Burma corresponds to the Pan-Xi Rift region.

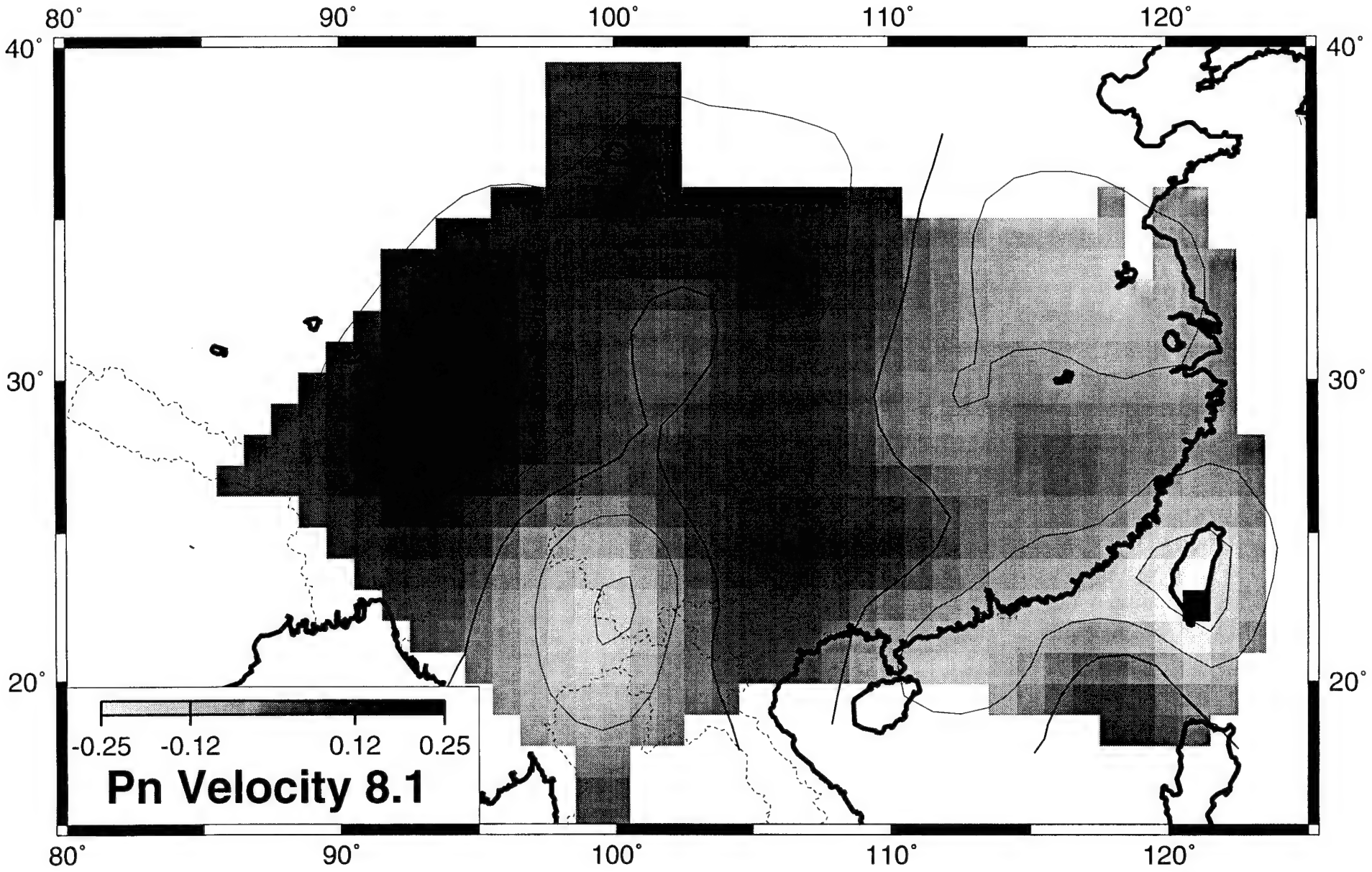

Figure 6c: Pn station delay times for Indochina. Due to the lack of data, the delays have high errors and are difficult to interpret.

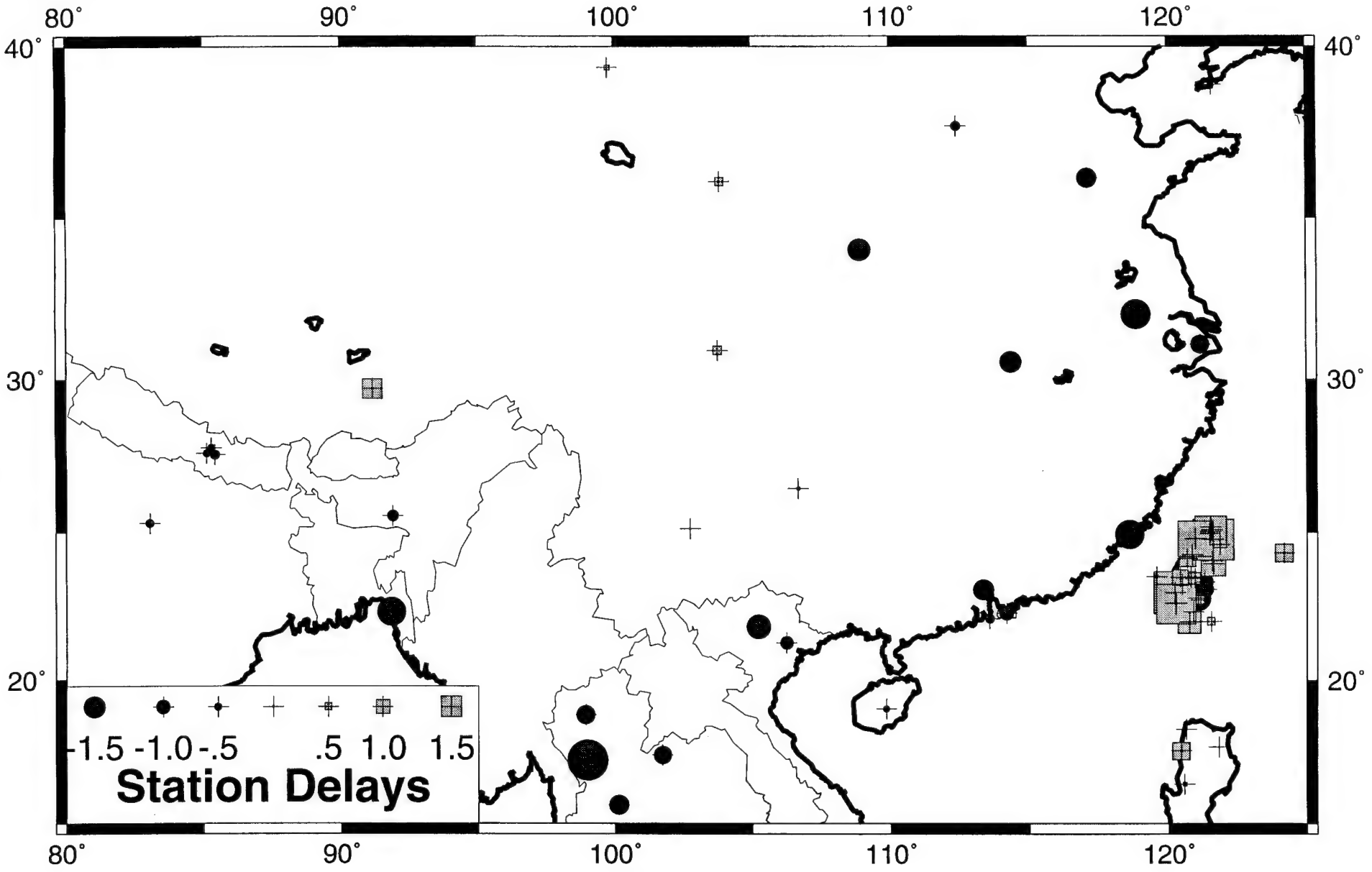

For the propagation efficiency measurements we used only event-station paths for which good three-component waveform data were available (Figure 7). All data were previewed for large signal to noise ratios and a P-wave arrival was picked on each vertical component. Horizontal components were decomposed into radial and transverse components. Vertical, radial and transverse seismograms were filtered with a two-pole, two-pass Butterworth filter with passband 0.5-5.0 Hz. We did not remove the instrument response or integrate the data, so all data were analyzed as raw velocity seismograms. We used the following group velocity windows to isolate each phase: P-wave (Pn and Pg) 8.0 km/s - 5.0 km/s; Sn 4.6 km/s - 4.1 km/s; and Lg 3.6 km/s - 3.0 km/s. Errors in some event locations and/or depths required us to manually pick these windows. Sn observations were restricted to the distance range 200-2600 km and Lg observations were restricted to the distance range of 200-3000 km. Once each phase was isolated, we computed the absolute amplitude of each windowed phase. The mean and absolute maximum value of each phase were found: P-wave on the vertical component, Sn on the transverse component and Lg on the vertical component. Amplitude ratios of the absolute mean value of Sn to the P-wave and the Lg to the P-wave were then computed. Figure 8 illustrates this procedure.

Amplitude ratios proved to be helpful for quantitatively assessing Lg propagation, however Sn propagation was difficult to assess purely by amplitude ratios. Thus, we subjectively ranked both Sn and Lg propagation (similar to previous studies with WWSSN data, e.g. Kadinsky-Cade et al, 1981). We used three categories: "efficient", "inefficient" and "not observed". For Sn, "efficient" propagation means that Sn is clearly observed as a group of waves arriving with group velocity of 4.5 km/s on the transverse component seismogram as a distinct arrival above the noise. Sn/P amplitude ratios were usually greater than 1.0 for efficient Sn paths, but were sometimes as low as 0.5. "Efficient" Sn was often emergent on continental paths and impulsive on oceanic paths. "Inefficient" Sn propagation means that Sn is detectable by the analyst as an emergent arrival within the specified group velocity window, sometimes accompanied by a shift to lower frequencies. Amplitude ratios for inefficient Sn propagation were scattered between 0.5-1.0. If Sn was not distinguishable from P-wave coda, then we classified the path as Sn "not observed". Similar classifications were used for Lg propagation. "Efficient" Lg propagation means that Lg was clearly observed on vertical and transverse component seismograms with Lg/P amplitude ratios greater than 1.5. "Inefficient" Lg propagation means that Lg was observed on vertical and transverse component seismograms, but weak. Lg/P amplitude ratios for "inefficient" Lg propagation were about 1.0. Lg was classified as "not observed" when Lg/P ratios were less than 0.5. Examples of Sn and Lg waveforms for stations in the Middle East are in Appendix A. Summary maps for Sn and Lg propagation efficien-

cies are in Figures 9 and 10 respectively. More detailed maps showing Sn and Lg efficiencies for raypaths to individual stations are in Appendix B (Sn) and Appendix C (Lg).

In the Middle East, Sn does not propagate over a region generally corresponding to the Turkish-Iranian Plateau (Figure 9). There, Sn is strongly attenuated even if the path is only a few hundred kilometers long. North of the Plateau, Sn propagates efficiently across the southern Caspian Sea, consistent with previous observations (Molnar and Oliver, 1969, and Kadinsky-Cade et al., 1981), and Sn also propagates efficiently along the northern flank of the Greater Caucasus Mountains, the Alborz Mountains, and the Koppeh Dagh. Our data does not provide tight constraints on the southern boundary of the Sn attenuation zone, but this boundary was well delineated by Kadinsky-Cade et al. (1981) as the Zagros Mountains and the new data supports this. Regions of low Pn velocity (Figure 3a) and those of poor Sn propagation efficiency (Figure 9) are strongly correlated. These regions also correlate well with regions of widespread continental volcanism (Figure 2) and this is consistent with the presence of partial melt in the uppermost mantle.

The efficient propagation of Lg across the stable shields and platforms of the Middle East is consistent with previous results and with data from other parts of the world (e.g. Ruzaikin et al., 1977; Kadinsky-Cade, 1981) and indicates both high Q and laterally uniform velocity structure in the stable continental crust. However, the tectonically active Turkish-Iranian Plateau shows weak Lg (Figure 10). We made measurements of Lg coda Q and found it to be low (200 to 400) (Wu, Ni, and Hearn (1995), consistent with what was previously found by Xie and Mitchell (1991) as well as the abundant recent volcanism on the Plateau (Dercourt et al., 1986; Pearce, et al., 1990). Geologic boundaries can also block Lg and it appears the abrupt changes in wave guide properties at the margin of the Turkish-Iranian Plateau are affecting the characteristics of Lg. Lg is rarely observed for paths crossing the Caucasus and Alborz Mountains. Paths that begin near the Zagros Mountains show observable Lg propagation. Gravity data from the Zagros indicate a gradual thickening of the crust to the north (Snyder and Barazangi, 1986) and is consistent with the observation of some observable Lg propagation there.

Regional Sn and Lg wave characteristics of western China

The Sn and Lg data analyses have been extended to the study of crust and mantle structure beneath the Tibet Plateau (Reese and Ni, 1996; Ni et al., 1995). Central to the studies are broadband data that were collected by the Chinese Digital Network (CDSN) (Figure 11). These data are augmented with data collected during two PASSCAL broadband experiments in Pakistan during 1993 and Tibet during

1994 (Ni et al., 1996). These field deployments were headed by New Mexico State University along with support from colleagues and local governments and funding from the National Science Foundation and the U.S. Agency for International Development. Data collected from these field experiments are important to seismology both because of the scientific interest in the Tibetan Plateau and because of two 1994 Lop Nor nuclear tests recorded by the Tibet experiment. Comparison between the Lop Nor nuclear events and a nearby earthquake shows that, at high frequencies (>1 Hz), both have similar spectrums and waveforms. However, at low frequencies the earthquake generates larger surface waves than the nuclear tests. In this report we only present Sn and Lg efficiencies for stations in western China; other stations and the data from Lop Nor are the subject of our continuing contract. A composite map of Sn propagation efficiency is shown in Figure 12. A similar map for Lg wave propagation efficiency is presented in Figure 13. Raypath maps of Sn and Lg propagation efficiencies for individual stations in China are in Appendix D

Sn propagates efficiently across the Himalayas to station LSA, Lhasa, Tibet (Figure 12). In contrast, Sn does not propagate through a large portion of central and northern Tibet. In southern Tibet, Sn propagation efficiency is reduced when compared with propagation paths traversing mainly the Himalayas. Sn is observed from crustal events originating in the western Himalayas, the Pamirs, and the Tien Shan to station WMQ, Urumqui, western China. Paths crossing the Tarim Basin to WMQ are all efficient. A few paths from eastern Tibet show efficient Sn propagation, but the majority of events in Tibet do not show Sn. The Mongolian Plateau does not allow Sn to propagate either. The zone of Sn blockage in northern Tibet corresponds to a region of low Pn velocity (~8.0 km/s) mapped by McNamara et al. (1996) and suggests that a small amount(<1%) of partial melt could exist there, possibly analogous with the mantle beneath the Turkish-Iranian Plateau or the Basin and Range Province.

Lg does not propagate efficiently (B and C classifications) across the Himalayas when the raypath is subparallel to the mountain range; however, it is observed for shorter raypaths that originate in the Indian Shield and are perpendicular to the strike of the mountain belt (Figure 13). However, events occurring in Burma do not propagate Lg across the Himalayas, but this may be related to the presence of the Pan-Xie rift in Burma. Within the Tibetan Plateau, Lg is observed only for paths with distances less than about 6 degrees. We also observed that the Indus-Tangpo Suture attenuates most crustal phases. The attenuation is probably due to a partially melted upper crust rather than the complex structure in the suture. Lg is observed for most raypaths, especially those raypaths that cross Mongolia, the Tien Shan Mountains, and the Tarim Basin. Lg is completely eliminated for a few of the longer paths crossing Tibet.

Figure 7: Map of the Middle East showing events and stations used to characterize Sn and Lg wave propagation in the region.

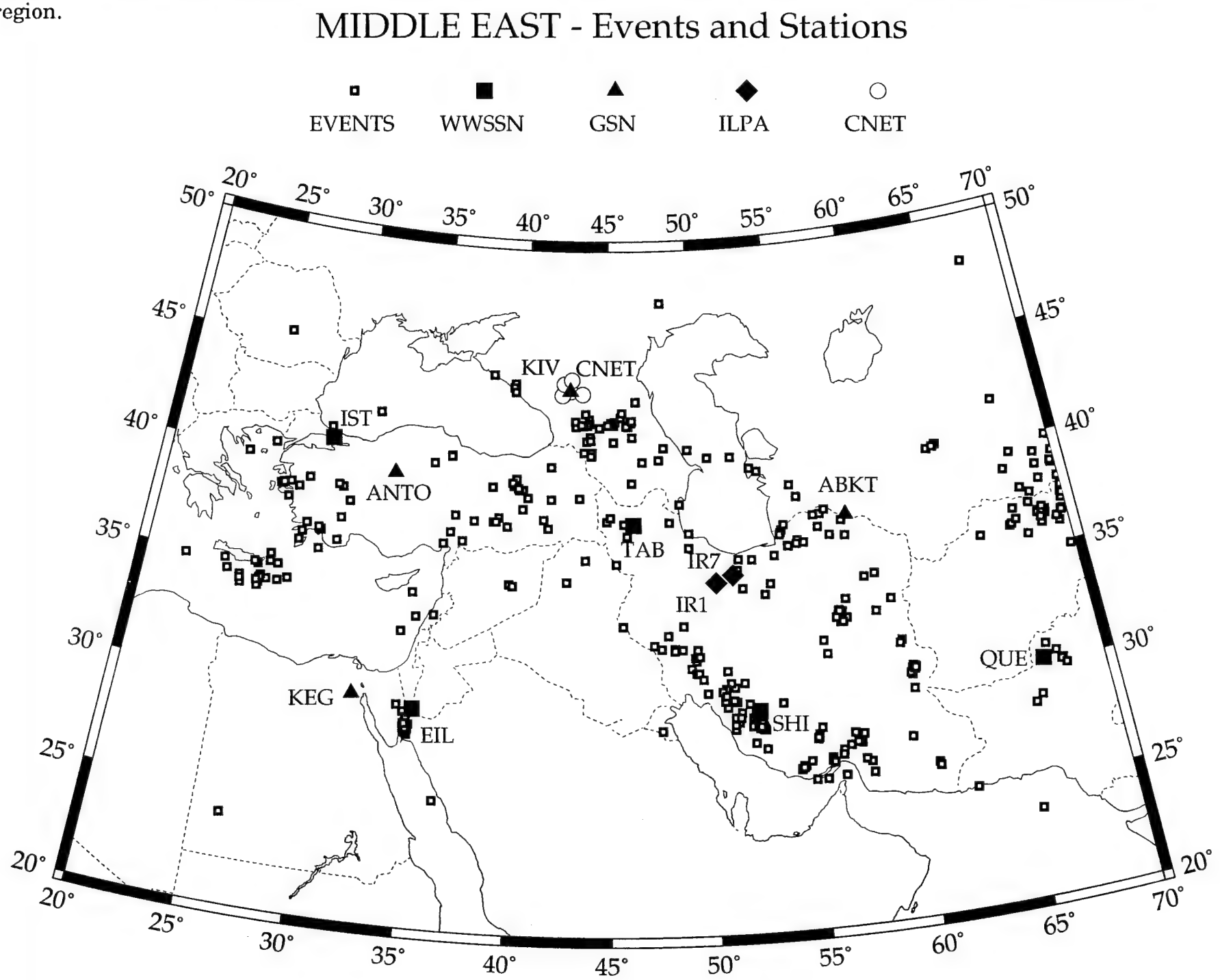

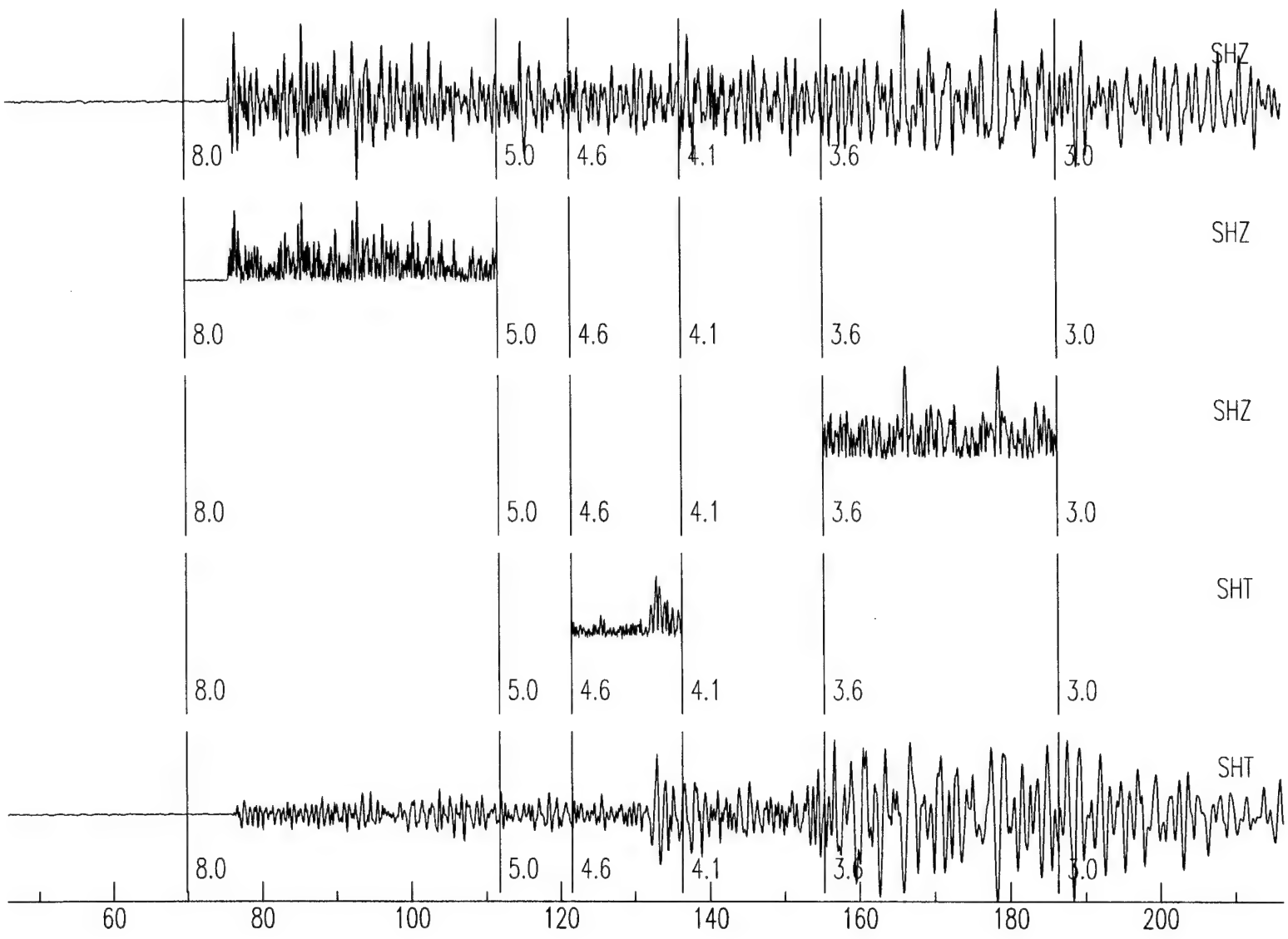

Figure 8: Illustration of the data analysis method for a raypath from the Zagros Mountains to ILPA station IR1 (distance 558.89 km, back-azimuth 178.24 degrees). Top: Filtered (0.5-5.0 Hz) vertical seismogram (SHZ). Velocity marks for 8.0, 5.0, 4.6, 4.1, 3.6, and 3.0 km/s are shown. Middle three: Absolute amplitudes for each window are shown. Bottom. Horizontal seismograph (SHT).

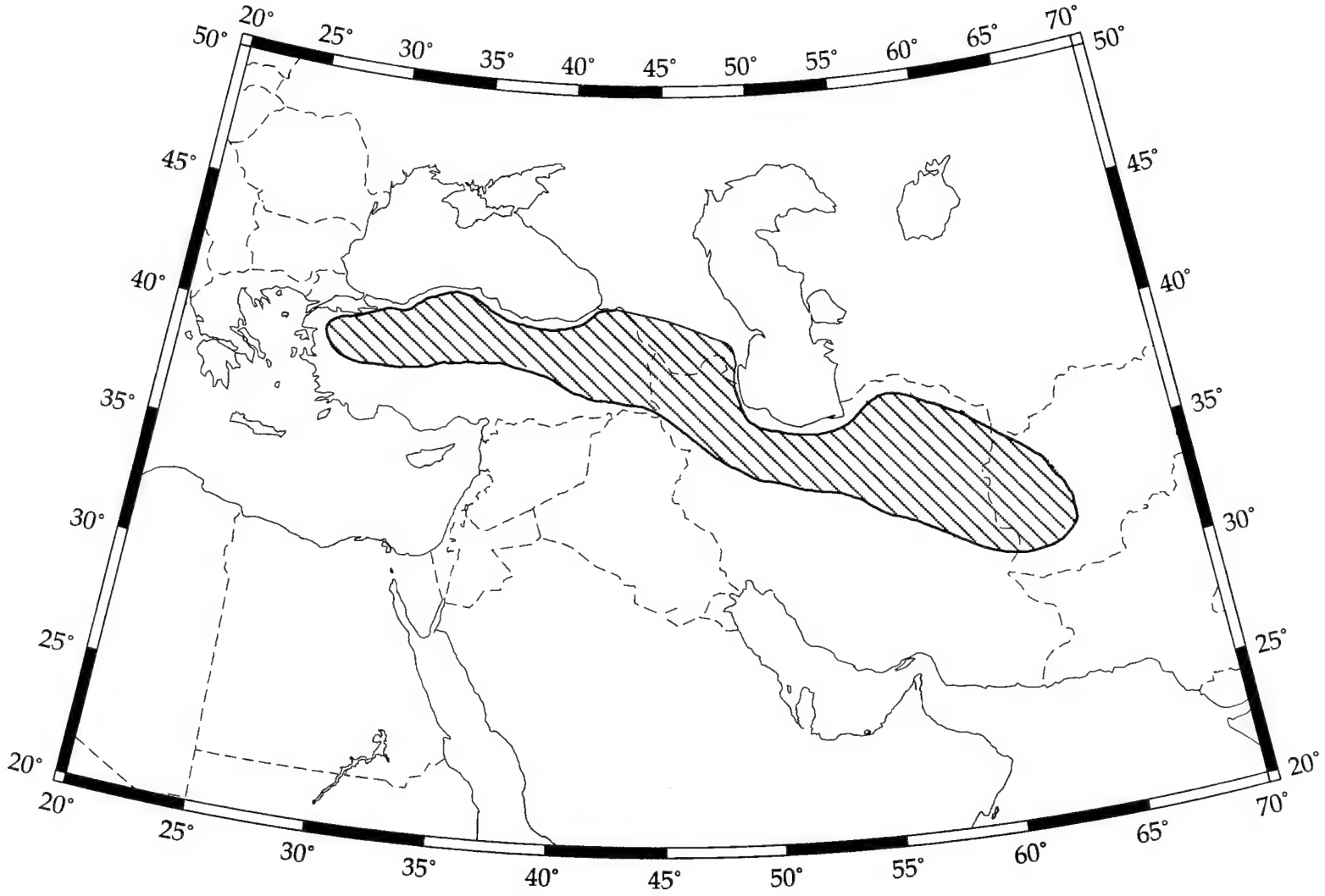

Figure 9: A map showing the region of Sn attenuation in the Turkish-Iranian Plateau. This region roughly corresponds to the zone of low Pn velocity of Figure 3b.

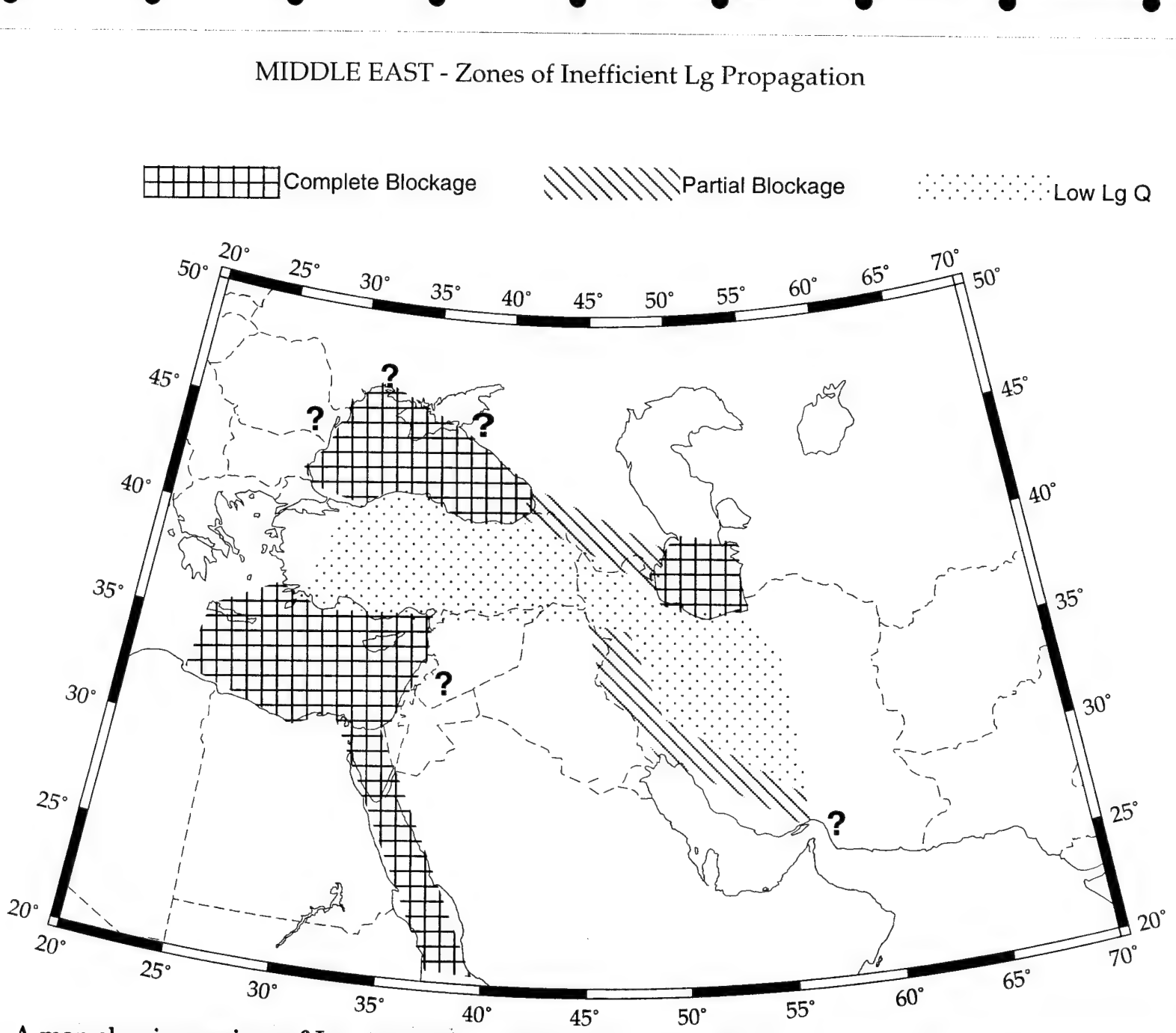

Figure 10: A map showing regions of Lg attenuation and blockage in the Turkish-Iranian Plateau. Cross-hatch pattern denotes areas of total Lg blockage; stripe pattern denotes areas of partial Lg blockage where Lg only occasionally propagates; dotted pattern denotes low Lg Q region where Lg propagates but shows clear attenuation.

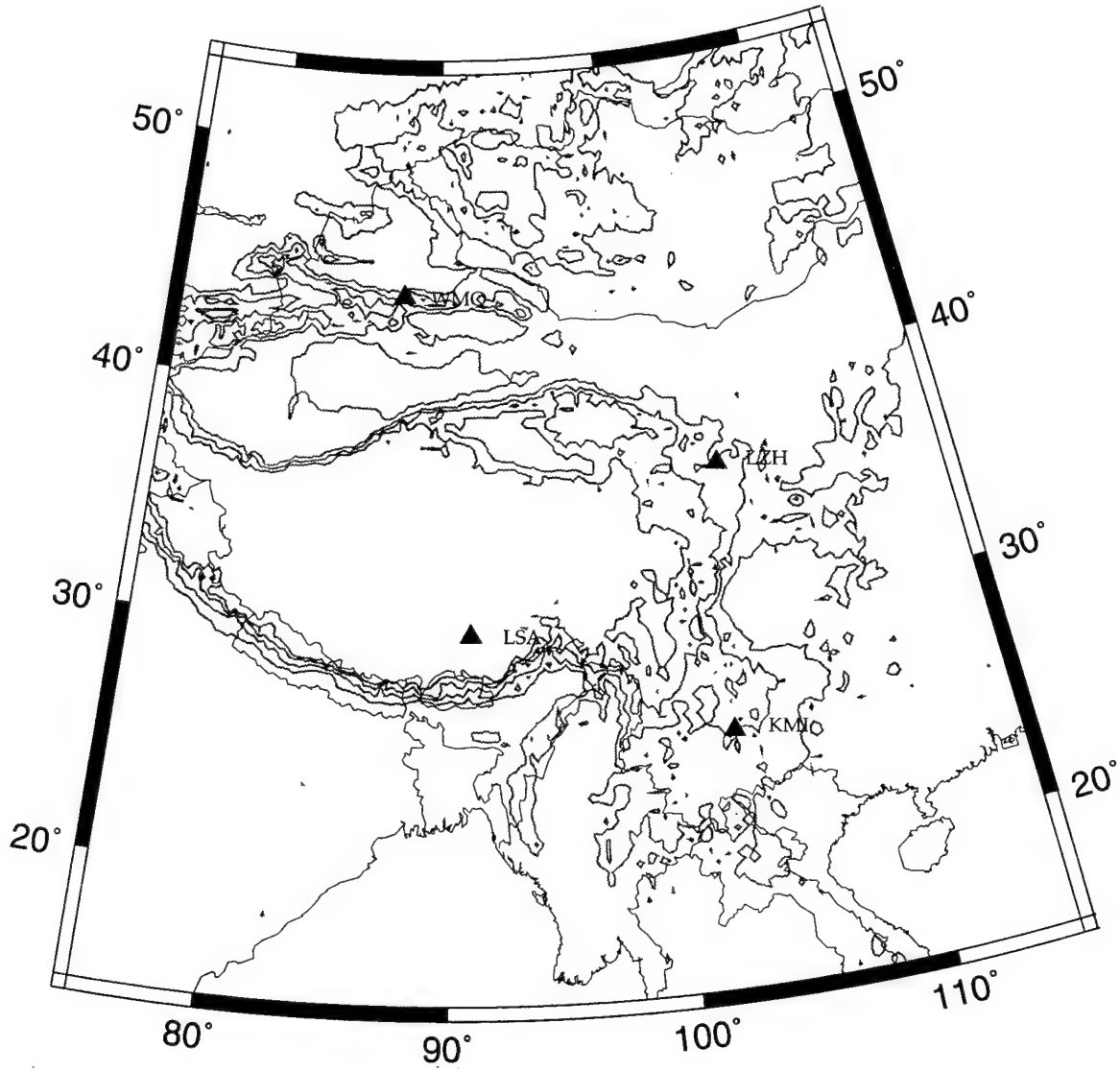

Figure 11: Map of China showing stations used for the Sn and Lg wave analyses. Contour level is 1000 m elevation.

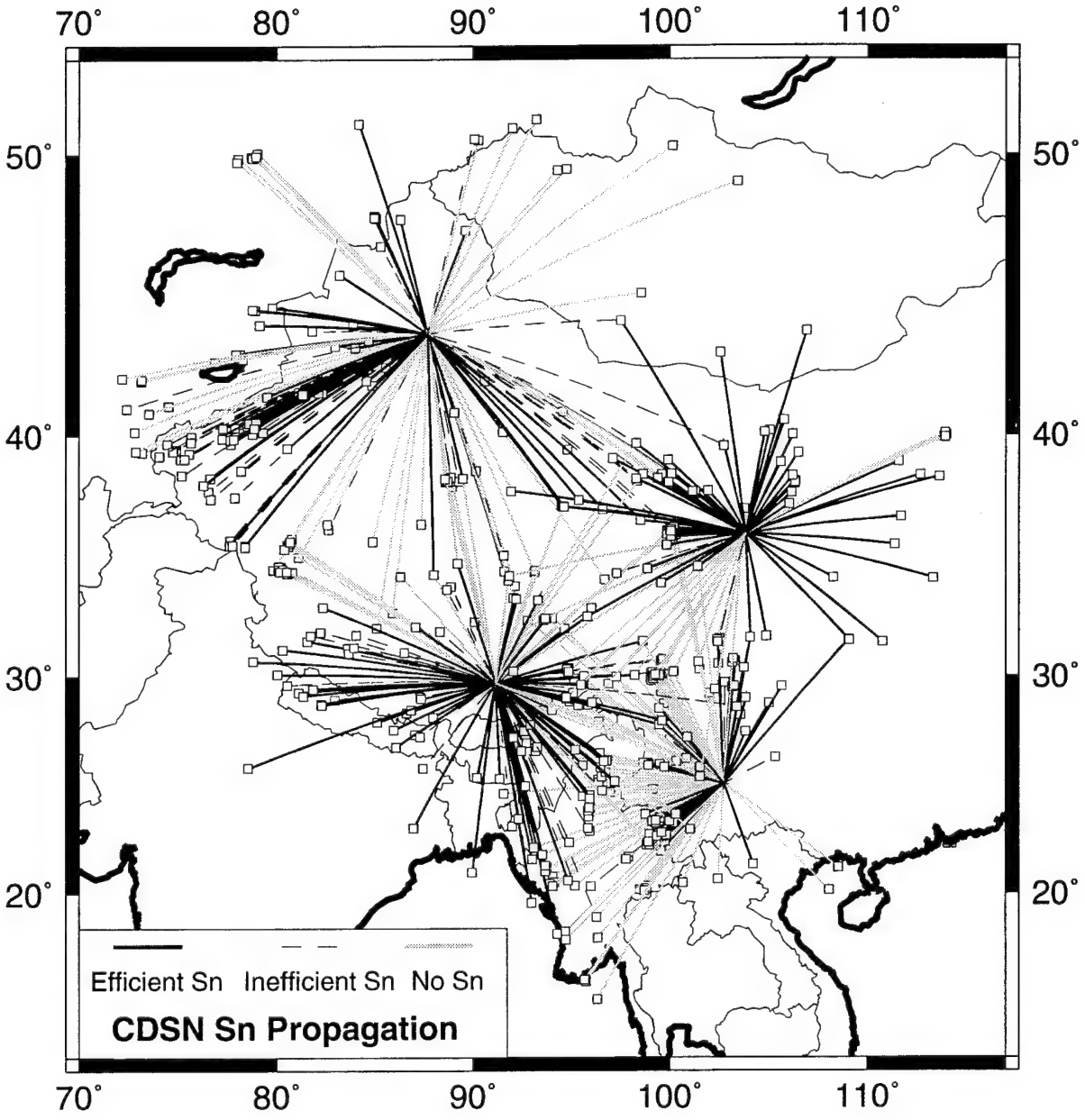

Figure 12: A summary map showing the efficiency of Sn wave propagation in China for all raypaths. Detailed maps are in Appendix D.

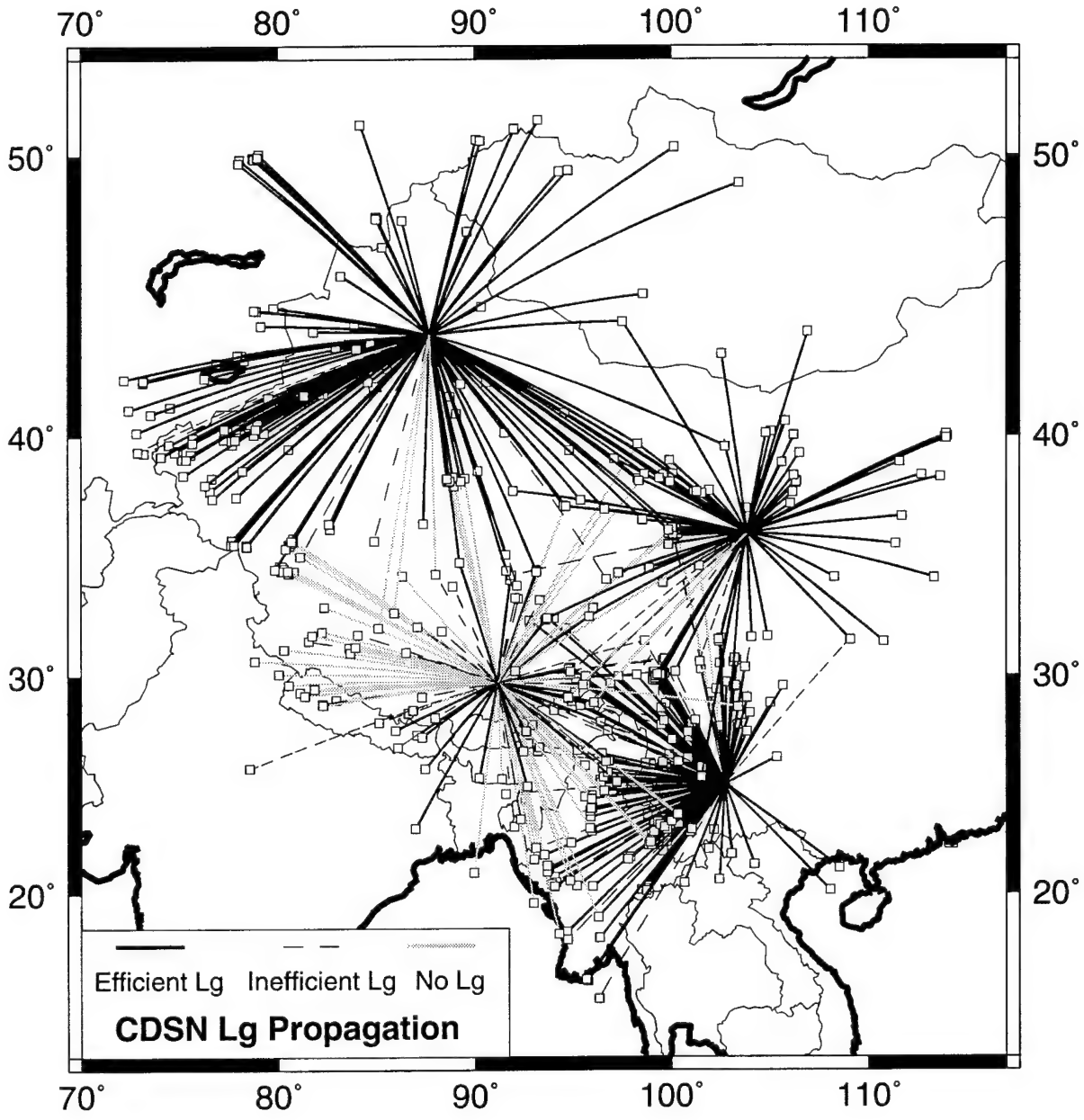

Figure 13: A summary map showing the efficiency of Lg wave propagation in China for all raypaths. Detailed maps are in Appendix D.

Conclusions

Results show that much of the southern Eurasian margin is underlain by hot, and, in some cases, partially melted mantle that developed during oceanic subduction episodes occurring prior to continental collision. The degree of partial melting could be exacerbated by the influx of water into the mantle from the subducting slab. This partial melting is well defined by zones of low Pn velocity. We find low Pn velocities for the collisional margins of the southern Mediterranean especially the Apennine Mountains of Italy, the Dinaride-Hellenide Mountain chain, and the Aegean Arc. These regions also have significant anisotropy oriented with the fast direction parallel to the arc. Low Pn velocity also exists beneath the Turkish-Iranian Plateau, the Hindu-Kush Mountains, and the Pan-Xie Rift.

For the Middle East, regions of low Pn velocity correlate to regions of Sn blockage and to the approximate boundaries of the Turkish-Iranian Plateau. This seismic structure is similar to that of the western United States and this, as well as the attenuated Lg wave propagation, suggests that nuclear discrimination methods developed for the western U.S. may be portable to the Turkish-Iranian Plateau. There is also a correspondence between low Pn velocity and no Sn propagation beneath northern Tibet. If such correlations can be extended to other paths of southern Eurasia, then Sn is also not expected to propagate for the southern Hindu-Kush Mountains or parts of Indochina. Good Sn propagation can be found for the Arabian Shield, the Russian Platform, and southern Tibet. Only for events occurring and recorded in these regions can Sn be of use in nuclear monitoring efforts.

The Lg phase also shows regional attenuation patterns. It propagates within geologic provinces, but is strongly attenuated within the Turkish-Iranian Plateau and the Tibetan Plateau. In general, Lg propagates even where the Sn phase does not. Major barriers to Lg are the oceanic structure of the Black Sea and the Caspian Sea, the Caucasus Mountains, Zagros Mountains, the Indus-Tangpo suture, and the Himalayas. Changes in crustal structure between at these province boundaries scatter the Lg phase. However, if stations can be situated within geologic provinces, Lg can be observed and used for regional nuclear monitoring.

Acknowledgments

We would like to thank Barbara Rueben of CSS for providing us with the raw ILPA data. The ILPA data was processed into CSS format event volume databases at the Joint Seismic Program Center of the University of Colorado, using codes written by Danny Harvey, Dan Quinlan and Michael Ritzwoller, to whom we are indebted. We thank Bob Engdahl for providing some event locations and origin times

inferred from ISC data. Map figures were made using GMT (Wessel and Smith, 1991).

References

Akasheh, B., Eshghi, I. and Soltanian, R., The Iranian Long-Period Array (ILPA), J. *Geophysics*, *42*, 159-162, 1976.

Beghoul, N., Barazangi, and B. Isacks, Lithospheric structure of Tibet and western North America: Mechanism of uplift and a comparative study, *J. Geophys. Res.*, *98*, 1997-2106, 1993.

Bouchon, M., Complete synthesis of seismic crustal phases at regional distances, *J. Geophys. Res., 87*, 1735-1741, 1982.

Chen, W., and Molnar, P., The uppermost mantle P wave velocities beneath Turkey and Iran, *Geophys. Res. Lett., 7*, 77-80, 1980.

Christensen, N. and Mooney, W., Seismic velocity structure and composition of the continental crust: A global view, *J. Geophys. Res.*, 100, 9761-9788, 1995.

Dercourt, J., Zonenshain, L., Ricou, L., Kazmin, V., Le Pichon, X., Knipper, A., Grandjacquet, C., Sbortshikov, I., Geyssant, J., Lepvrier, C., Pechersky, D., Boulin, J., Sibuet, J., Savostin, L., Sorokhtin, O., Westphal, M., Bazhenov, M., Lauer, J., and Biju-Duval, B., Geological evolution of the Tethys Belt from the Atlantic to the Pamirs since the Lias, *Tectonophysics, 123*, 241-315, 1986.

Hearn, T. M., Pn Traveltimes in Southern California, *Journal of Geophysical Research*, *89*, 1843-1855, 1984.

Hearn, T. Anisotropic Tomography in the Western United States, submitted to the *Journal of Geophysical Research*, *101*, 8403-8414, 1996.

Hearn, T., and J. Ni, Pn Tomography of Southern Europe from Pn Data, *EOS Trans Am Geophys Union*, *72*, number 44, page 349, presented at the December 1991 American Geophysical Union Meeting, 1991.

Hearn, T., and J. Ni, Pn Travel-Time Tomography of Eurasia, *Seismological Research Letters*, *v63*, n1, p27, 1992, presented at the April 1992 Seismological Society of America Meeting, Santa Fe, New Mexico, 1992a.

Hearn, T., and J. Ni, Low Pn Velocity and the Turkish-Iran Plateau, *EOS Trans Am Geophys Union*, *v73*, n14, p209, April 1992, presented at the 1992 Spring American Geophysical Union Meeting, May 1992, Montreal, Canada, 1992b.

Hearn, T., and J. Ni, Low Uppermost Mantle Velocity Beneath the Western Hindu-Kush Range, *EOS Trans. Am. Geophys. Union*, *v73*, n43, p408, Oct. 27 1992, presented at the 1992 Fall American Geophysical Union Meeting, December 1992, San Francisco, CA, 1992c.

Hearn, T., and Ni, J., Pn velocities beneath continental collision zones: the Turkish-Iranian Plateau, *Geophys. J. Int.*, *117*, 273-283, 1994.

Hearn, T. and J. Wu, Pn Anisotropy beneath Southern Europe, *EOS Trans. AGU*, *76*, 46, pF413, 1995.

Hearn, T. and J. Wu, Anisotropic Pn Tomography beneath Southern Europe, in preparation for *Geophysical Journal International*, 1996.

Kadinsky-Cade, K., Barazangi, M., Oliver, J. and Isacks, B., Lateral variations in high-frequency seismic wave propagation at regional distances across the Turkish and Iranian Plateaus, *J. Geophys. Res., 86*, 9377-9396, 1981.

Kennett, B., Lg waves and structural boundaries, *Bull. Seism. Soc. Am., 76*, 1133-1141, 1986.

McNamara, D., Owens, T., and Walter, W., Observations of regional phase propagation across the Tibetan Plateau, *J. Geophys. Res., 100*, 22, 215-22, 229, 1995.

McNamara, D., W. Walter, T. Owens, and C. Ammon, Upper mantle velocity structure beneath the Tibetan Plateau from Pn travel time tomography, *J. Geophys. Res.*, in press, 1996.

Mele, G., M. Barazangi , T. Hearn, A. Rovelli, and D. Seber , High-frequency Seismic Wave Propagation in the Uppermost Mantle beneath Italy, International Union of Geodesy and Geophysics XXI General Assembly, July 2-14, 1995.

Molnar, P. and Oliver, J., Lateral variations of attenuation in the upper mantle and discontinuities in the lithosphere, *J. Geophys. Res.*, 74, 2648-2682, 1969.

NEIC (National Earthquake Information Center), *ISC Bulletin*, Compact Disk published by NEIC, Denver, Colorado, 1990.

Ni, J. and Barazangi, M., High-frequency seismic wave propagation beneath the Indian Shield, Himalayan Arc, Tibetan Plateau and the surrounding regions: High uppermost mantle velocities and efficient Sn propagation beneath Tibet, *Geophys. J. R. Astro. Soc., 72*, 665-689, 1983.

Ni, J., R. Rapine, J. Wu, and T. Hearn, Regional wave propagation characteristics in China and southern Asia, 17th Annual Seismic Research Symposium, Sept. 11-15, Scottsdale, Az., 1995.

Ni, J. and 11 others, Results from the INDEPTH-II passive source experiment: Implications for underthrusting of the Indian continental lithosphere beneath southernmost Tibet, submitted to Science, 1996.

Nuttli, O., 1980. The excitation and attenuation of seismic crustal phases in Iran. *Bull. Seism.. Soc. Amer., 70*, 469-485, 1980.

Pearce, J., J. Bender, , S. De Long, W. Kidd, P. Low, Y. Guner, F. Saroglu, Y. Yimaz, S. Moorbath, and J. Mitchell, Genesis of collision volcanism in Eastern Anatolia, Turkey, *J. Volcanol. Geoterm. Res., 44*, 189-229, 1990.

Press, F. and Ewing, M., 1952. Two slow surface waves across North America, *Bull. Seism. Soc. Amer., 42*, 219-228, 1952.

Rapine, R., J. Ni, and T. Hearn, Sn and Lg wave propagation in China, in preparation for the *Bulletin of the Seismological Society of America*, 1996.

Rapine, R, J. Wu, J. Ni, T. Hearn, Regional Sn and Lg wave propagation efficiencies in China, Indochina, and Mongolia, *EOS Trans. AGU, 76*, 46, pF428, 1995.

Reese, C., and J. Ni, Attenuation of coda waves in southern Tibet, submitted to Geophys. Res. Lett., 1996.

Rodgers, A., T. Hearn, and J. Ni, July 1994. Uppermost Mantle Structure in Southern Eurasia from Pn Tomography and Sn Attenuation, paper for the 16th Annual Seismic Research Symposium, Thornewood, NY, September 1994.

Rodgers, A., T. Hearn, and J. Ni, Pn, Sn, and Lg Propagation in the Middle East, *EOS Trans Am Geophys Union, 75*, 463, presented at the December, 1994 American Geophysical Union Meeting, San Francisco, CA, 1994.

Rodgers, A., J. Ni, and T. Hearn, Pn, Sn and Lg propagation in the Middle East, submitted to the *Bulletin of the Seismological Society of America*, 1996.

Ruzaikin, A., I Nersesov, V. Khalturin, V, and P. Molnar, Propagation of Lg, and lateral variations in crustal structure in Asia, *J. Geophys. Res., 82*, 307-316.

Sato, H., Sacks, I., and Murase, T., The use of laboratory data for estimating temperature and partial melt fraction in the low velocity zone: Comparison with heat flow and electrical conductivity studies, *J. Geophys. Res., 94*, 5689-5704, 1989.

Snyder, D., and Barazangi, M., Deep crustal structure and flexure of the Arabian Plate beneath the Zagros collisional mountain belt as inferred from gravity observations, *Tectonics, 5*, 361-373. 1986.

Spakman, W., Delay-time tomography of the upper mantle below Europe, the Mediterranean and Asia Minor, *Geophys. J. Int.*, **107**, 309-332, 1991.

Wessel, P. and Smith, W., Free software helps display data, *EOS Trans. Amer. Geophys. U. 72*, 441, 445-446, 1991.

Wu, J., J. Ni, and T. Hearn, Lg wave attenuation and propagation characteristics in Iran, in *Monitoring a Comprehensive Test Ban Treaty*, NATO ASI Volume, Eds., E. Husebye and A. Dainty, 655-662, Kluwer Academic Publishers, 1996.

Xie, J., and B. Mitchell, Lg coda Q across Eurasia, in yield and discrimination studies in stable continental regions, B. Mitchell (ed). Report PL-TR-91-2286, Phillips Laboratory, Hanscom Air Force Base, MA, 77-91, 1991.

Publications with support from this contract

Reviewed publications

Hearn, T. and J. Wu, Anisotropic Pn Tomography beneath Southern Europe, in preparation for *Geophysical Journal International*, 1996.

Rapine, R., J. Ni, and T. Hearn, Sn and Lg wave propagation in China, in preparation for the *Bulletin of the Seismological Society of America*, 1996.

Rodgers, A., J. Ni, and T. Hearn, Pn, Sn and Lg propagation in the Middle East, submitted to the *Bulletin of the Seismological Society of America*, 1996.

Wu, Jianxin, J. Ni, and T. Hearn, Lg wave attenuation and propagation characteristics in Iran, in *Monitoring a Comprehensive Test Ban Treaty*, NATO ASI Volume, Eds., E. Husebye and A. Dainty, 655-662, Kluwer Academic Publishers, 1996.

Hearn, T., and Ni, J., 1994. Pn velocities beneath continental collision zones: The Turkish-Iranian Plateau, *Geophys. J. Int.*, 117, 273-283.

Conference proceedings

Ni, J., R. Rapine, J. Wu, and T. Hearn, Regional wave propagation characteristics in China and southern Asia, 17th Annual Seismic Research Symposium, Sept. 11-15, Scottsdale, Az., 1995.

Reese, C., J. Ni and T. Hearn, Scattering attenuation in fractally homogeneous Random media, 17th Annual Seismic Research Symposium, Sept. 11-15, Scottsdale, Az, 1995.

Rodgers, A., T. Hearn, and J. Ni, July 1994. Uppermost Mantle Structure in Southern Eurasia from Pn Tomography and Sn Attenuation, paper for the 16th Annual Seismic Research Symposium, Thornewood, NY, September 1994. This paper will be presented as a poster at the symposium, 1994.

Meeting abstracts presented

Rapine, R, J. Wu, J. Ni, T. Hearn, Regional Sn and Lg wave propagation efficiencies in China, Indochina, and Mongolia, *EOS Trans. AGU*, 76, 46, pF428, 1995.

Hearn, T. and J. Wu, Pn Anisotropy beneath Southern Europe, *EOS Trans. AGU*, 76, 46, pF413, 1995.

Mele, G., M. Barazangi , T. Hearn, A. Rovelli, and D. Seber , High-frequency Seismic Wave Propagation in the Uppermost Mantle beneath Italy, International Union of Geodesy and Geophysics XXI General Assembly, July 2-14, 1995.

Wu, J., J. Ni, and T. Hearn, Lg Wave Attenuation and Propagation Characteristics in Iran, *Seismological Research Letters*, 66, 2, 51, 1995.

Rodgers, A., T. Hearn, and J. Ni, Pn, Sn, and Lg Propagation in the Middle East, *EOS Trans Am Geophys Union*, 75, 463, presented at the December, 1994 American Geophysical Union Meeting, San Francisco, CA.

Hearn, T., A. Rodgers, and J. Ni, Uppermost Mantle Structure in Southern Eurasia from Pn Tomography and Sn Attenuation, short abstract for presentation at the Seismic Research Symposium, Thornewood NY, Sept. 7-9, 1994.

Hearn, T., and J. Ni, Low Uppermost Mantle Velocity Beneath the Western Hindu-Kush Range, *EOS Trans Am Geophys Union*, v73, n43, p408, Oct. 27 1992, presented at the 1992 Fall American Geophysical Union Meeting, December 1992, San Francisco, CA.

Hearn, T., and J. Ni, Low Pn Velocity and the Turkish-Iran Plateau, *EOS Trans Am Geophys Union*, v73, n14, p209, April 1992, presented at the 1992 Spring American Geophysical Union Meeting, May 1992, Montreal, Canada.

Hearn, T., and J. Ni, Pn Travel-Time Tomography of Eurasia, *Seismological Research Letters*, v63, n1, p27, 1992, presented at the April 1992 Seismological Society of America Meeting, Santa Fe, New Mexico.

Hearn, T., and J. Ni, Pn Tomography of Southern Europe from Pn Data, *EOS Trans Am Geophys Union*, vol 72, number 44, page 349, presented at the December 1991 American Geophysical Union Meeting.

Personnel

Principle Investigators:

Thomas M. Hearn, Assistant Professor, Physics Dept., New Mexico State University. Geophysics Ph.D. Caltech 1985, Geophysics, Thesis: Crustal Structure in Southern California from Array Data. Geophysics M.S. Caltech 1982.

James F. Ni, Professor, Earth Sciences Ph.D. Cornell, 1984, Thesis: Seismicity and Active Tectonics of the Himalayas and Tibet. Civil and Environmental Engineering M. Engr. 1973.

Graduate Students and Postdoctoral Associates:

Richard Rapine, Graduate Student, Physics Dept., New Mexico State University.

Chris Reese, Graduate Student, Physics Dept., New Mexico State University.

Arthur Rodgers, Postdoctoral Associate, Physics Dept., New Mexico State University. Physics, 1994. Ph.D. University of Colorado 1993, Thesis: Tomographic Imaging of Internal Earth Structure: The Core-Mantle boundary and the Trade-off between Volumetric and Topographic Structure. Physics M.S. 1988. Now at University of California at Santa Cruz, Department of Earth Sciences.

Jianxin Wu, Graduate Student / Postdoctoral Associate, Physics dept., New Mexico State University. Ph.D., New Mexico State University, 1995.

Outside Collaborators (on the tomography of Italy):

Muawia Barazangi, Senior Research Scientist, Cornell University, Ithaca, NY.

Giuliana Mele, Graduate Student, Instituto Nazionale di Geofisica, Rome, Italy.

Dogan Seber, Graduate Student / Postdoctoral Associate, Cornell University, Ithaca, NY.

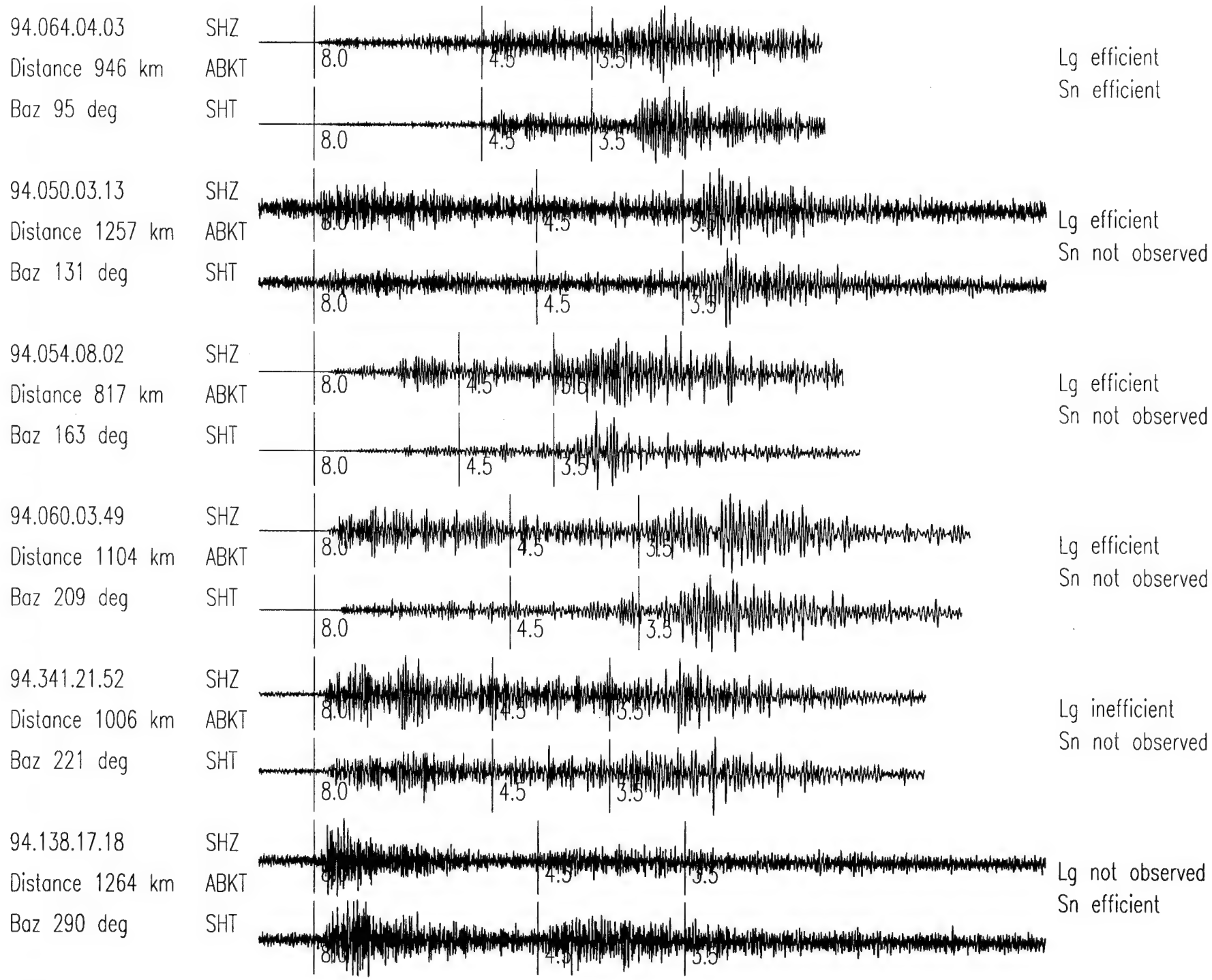

Figure A1: Example seismograms for station ABKT.

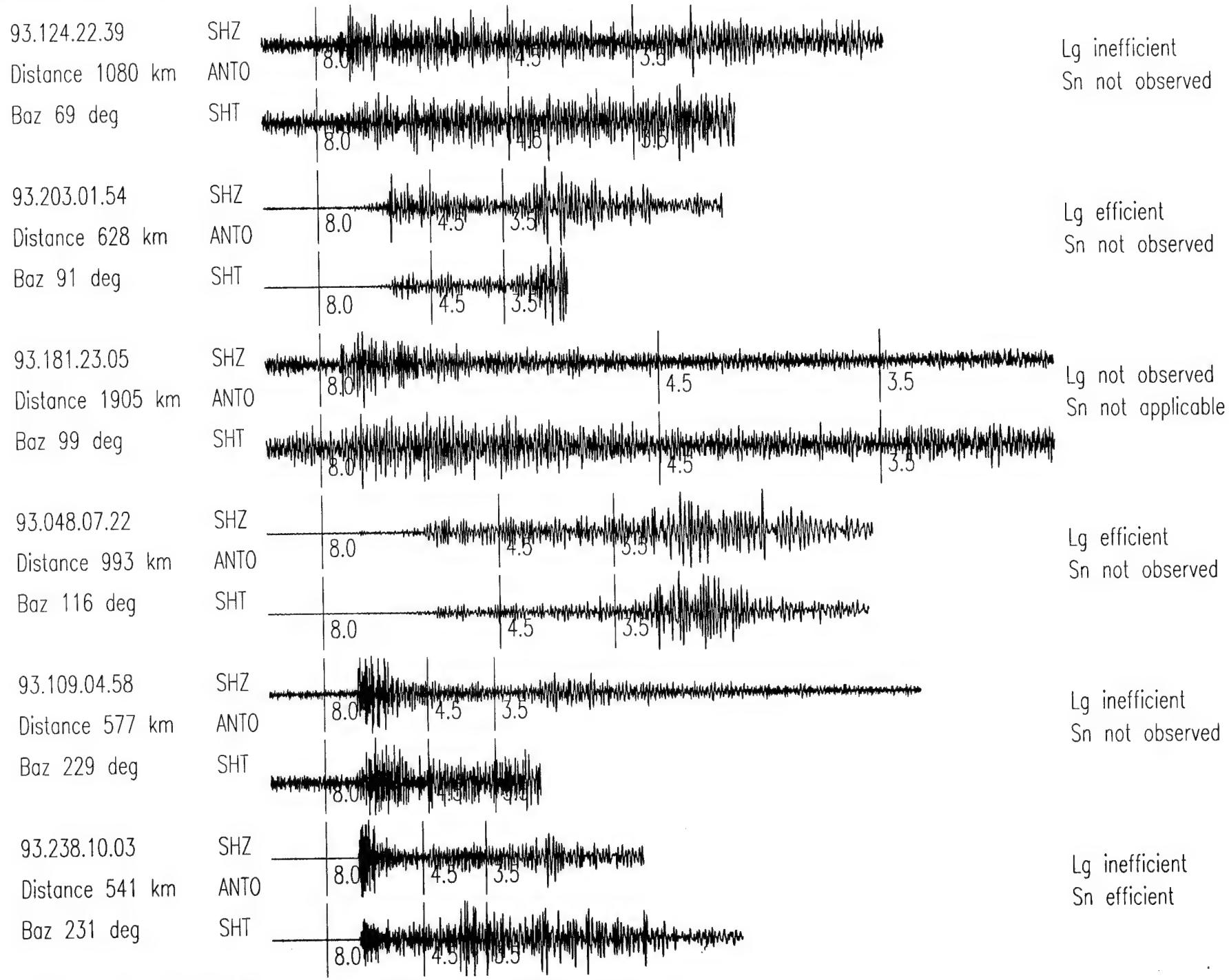

Figure A2: Example seismograms for station ANTO.

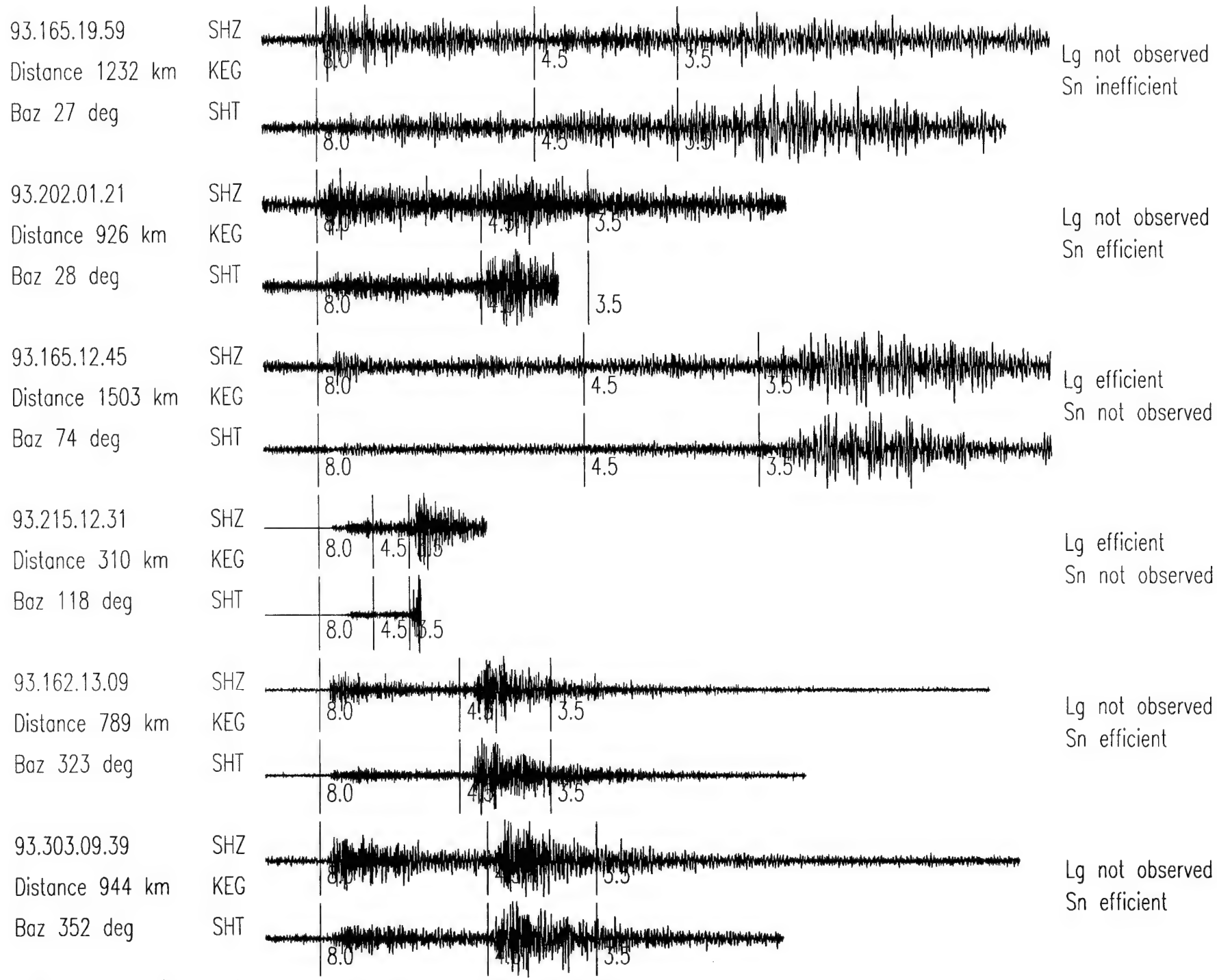

Figure A3: Example seismograms for station KEG.

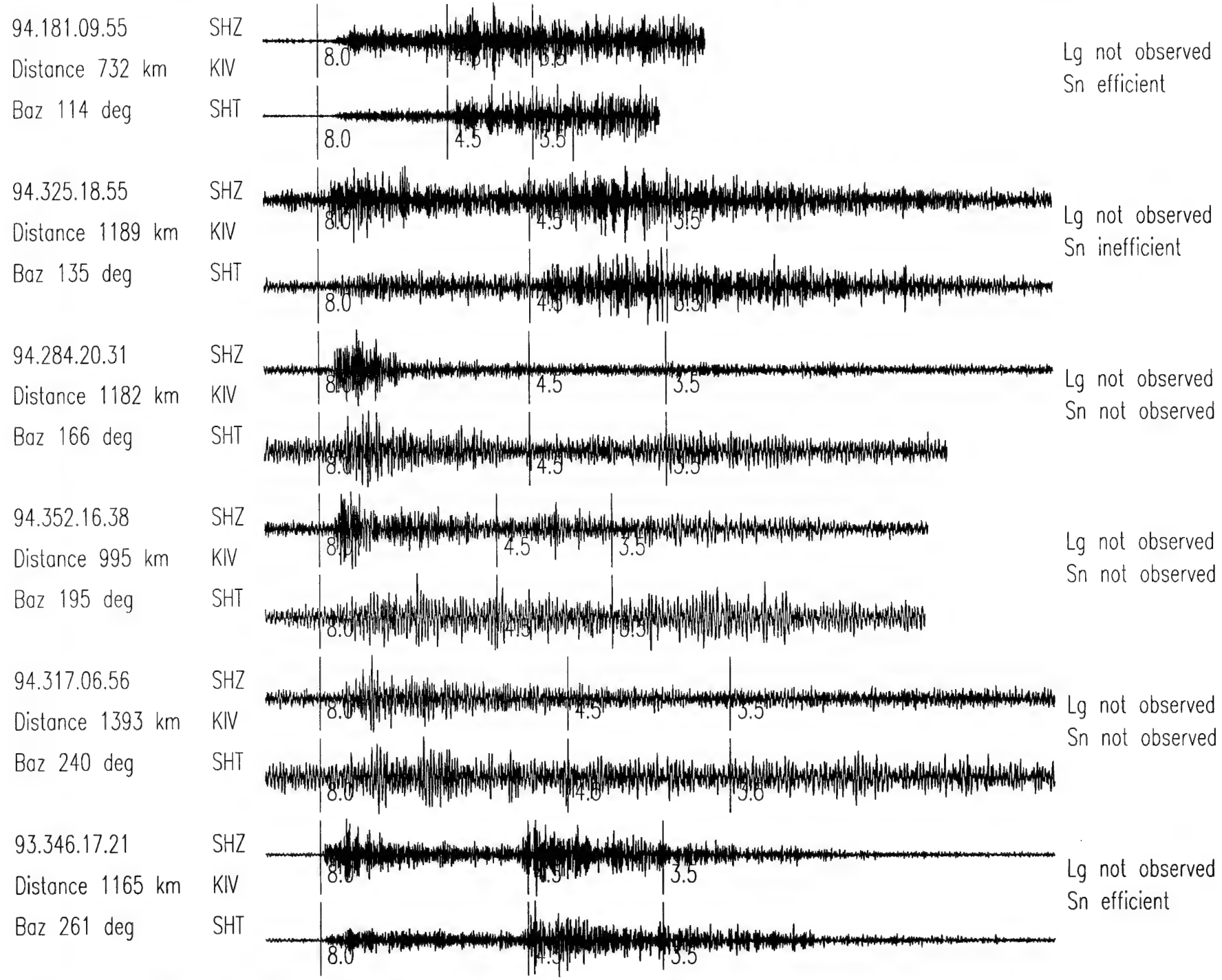

Figure A4: Example seismograms for station KIV.

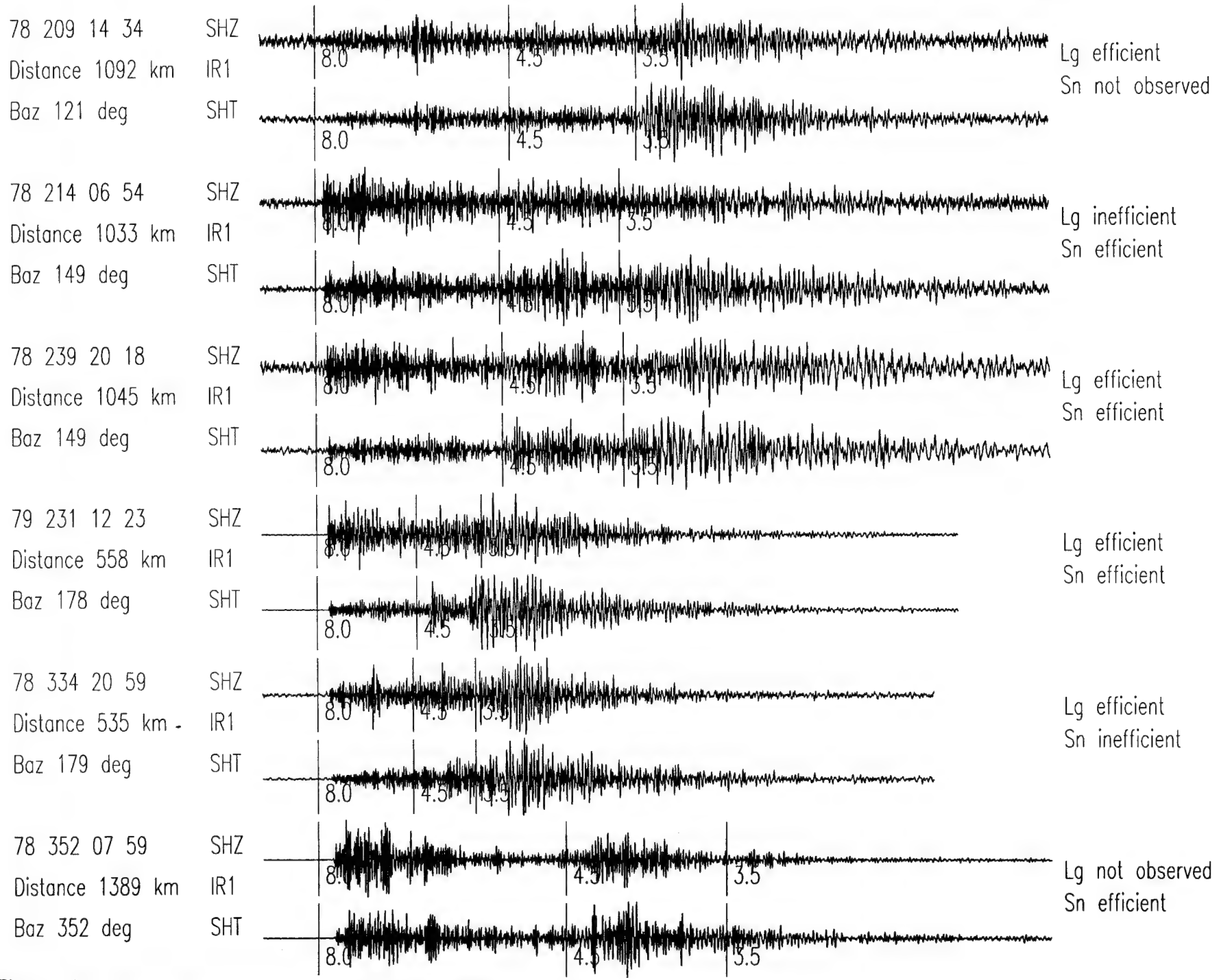

Figure A5: Example seismograms for station IR1 at ILPA.

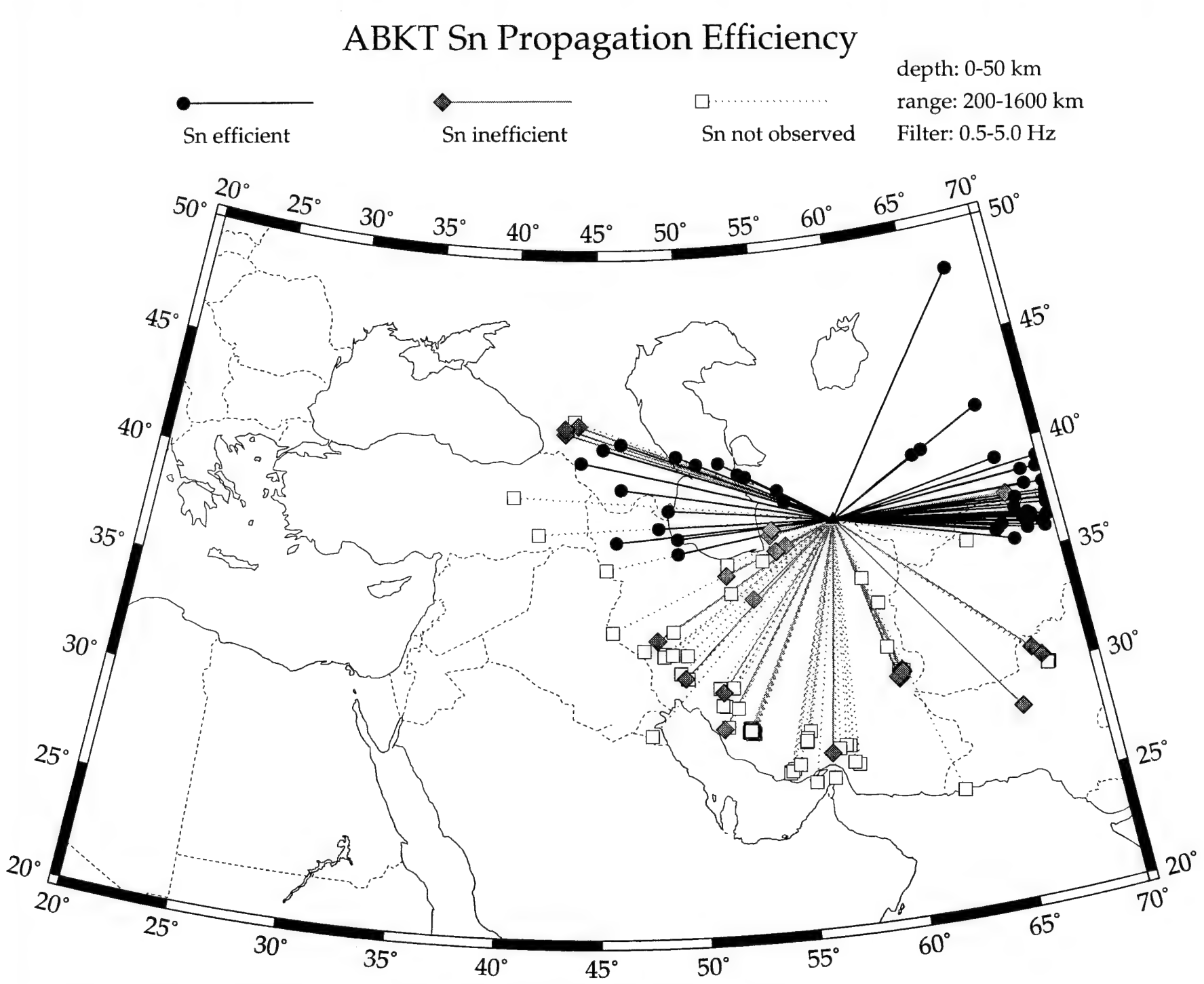

Figure B1: Map showing the efficiency of Sn wave raypaths at station ABKT.

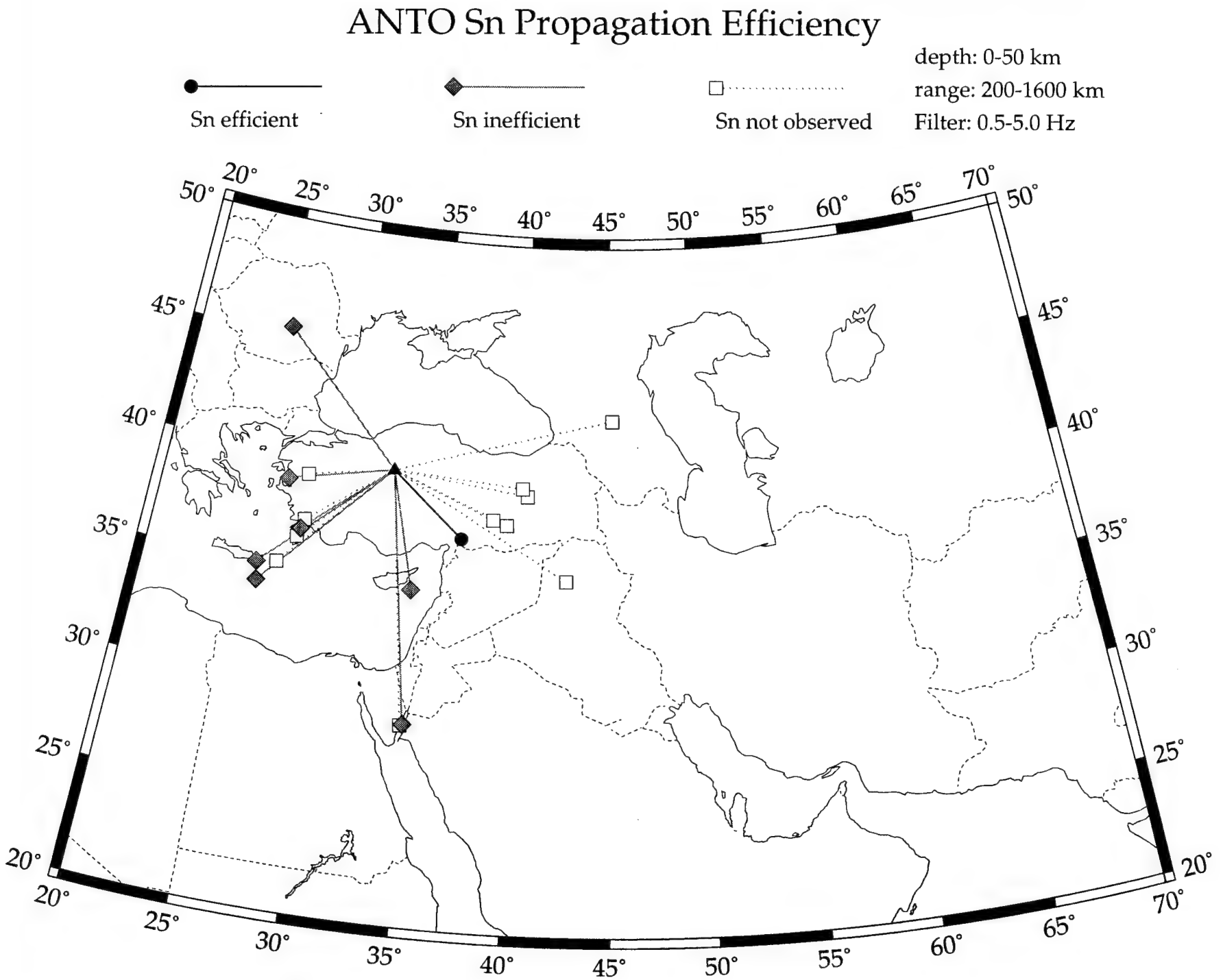

Figure B2: Map showing the efficiency of Sn wave raypaths at station ANTO.

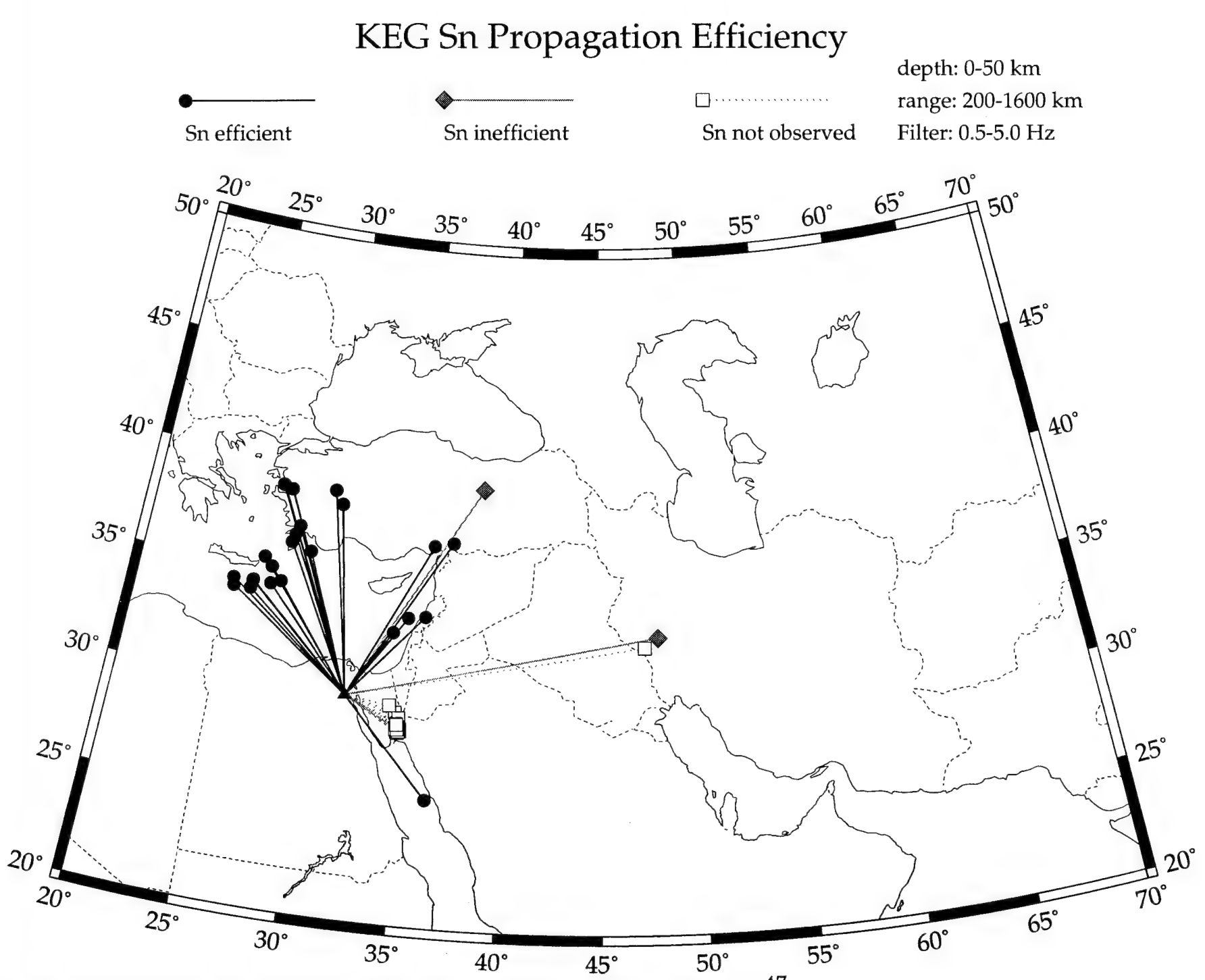

Figure B3: Map showing the efficiency of Sn wave raypaths at station KEG.

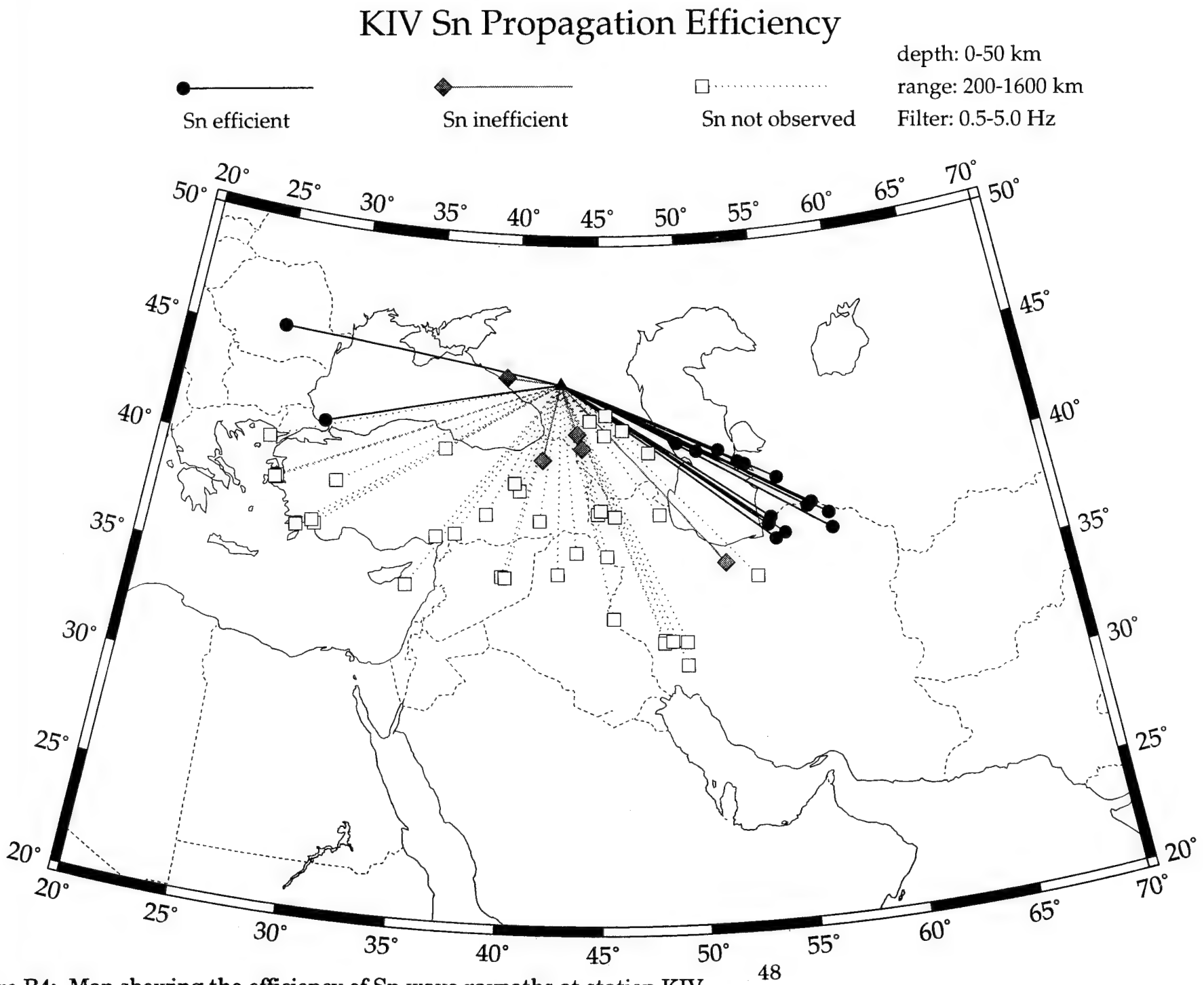

Figure B4: Map showing the efficiency of Sn wave raypaths at station KIV.

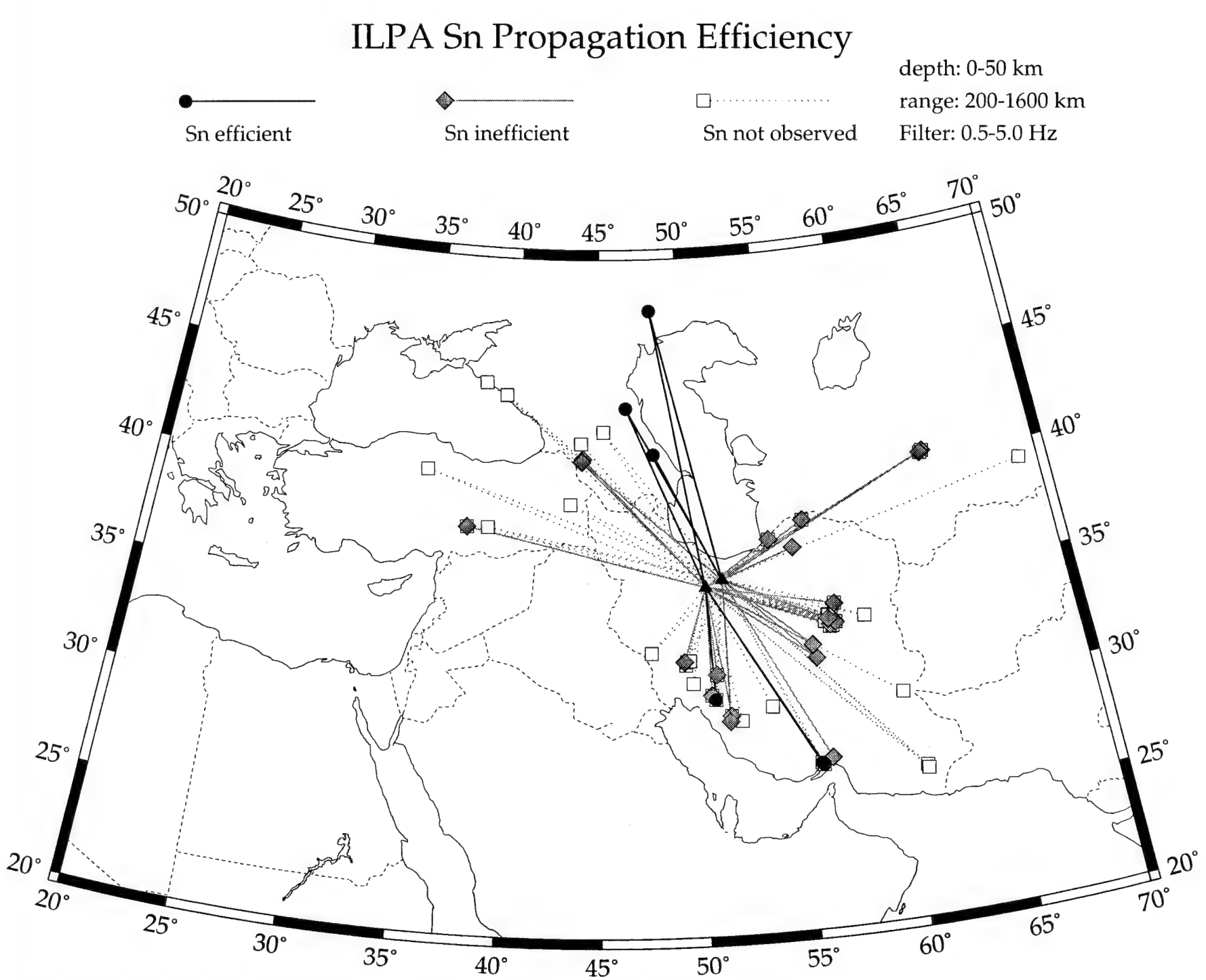

Figure B5: Map showing the efficiency of Sn wave raypaths at ILPA stations.

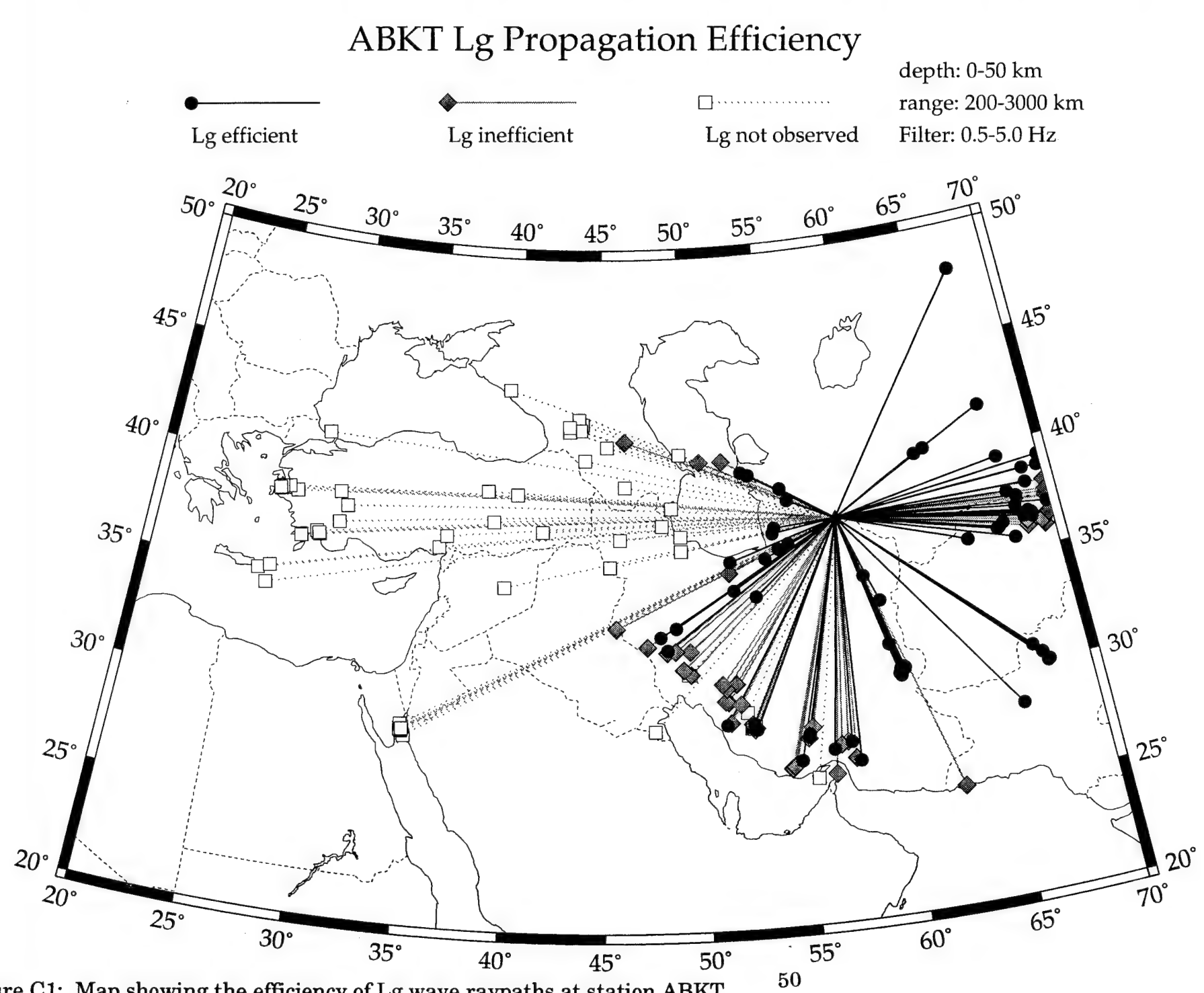

Figure C1: Map showing the efficiency of Lg wave raypaths at station ABKT.

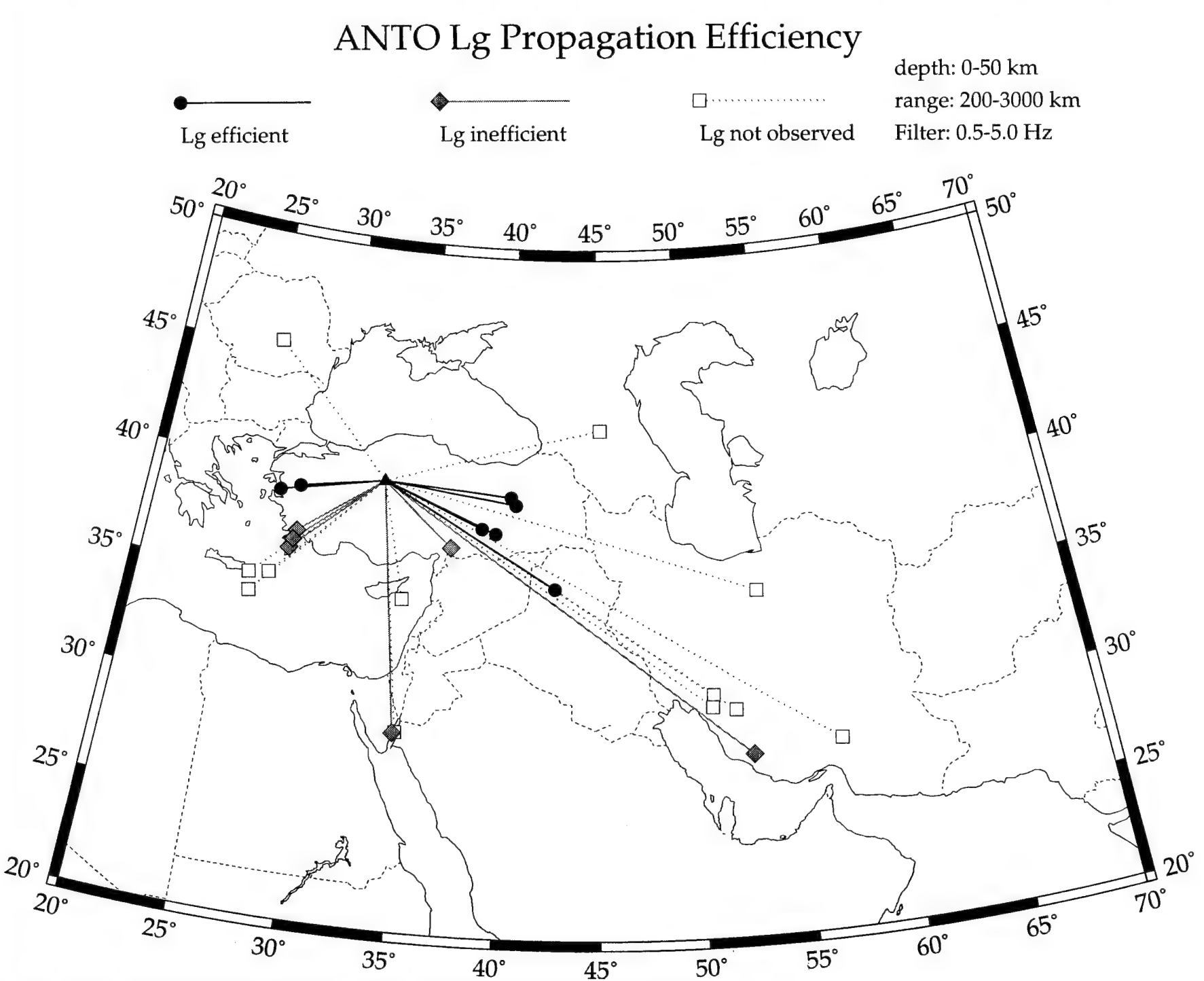

Figure C2: Map showing the efficiency of Lg wave raypaths at station ANTO.

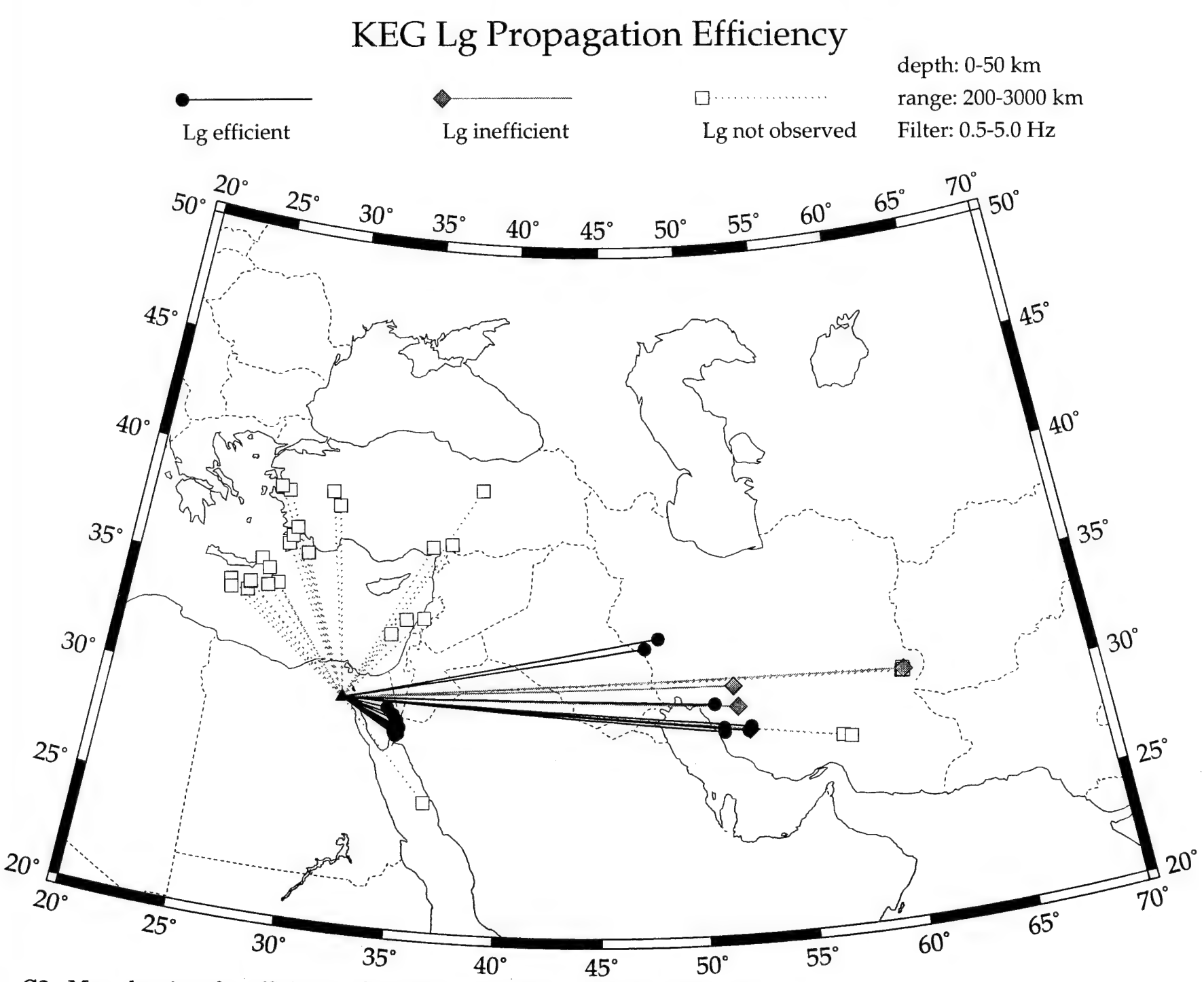

Figure C3: Map showing the efficiency of Lg wave raypaths at station KEG.

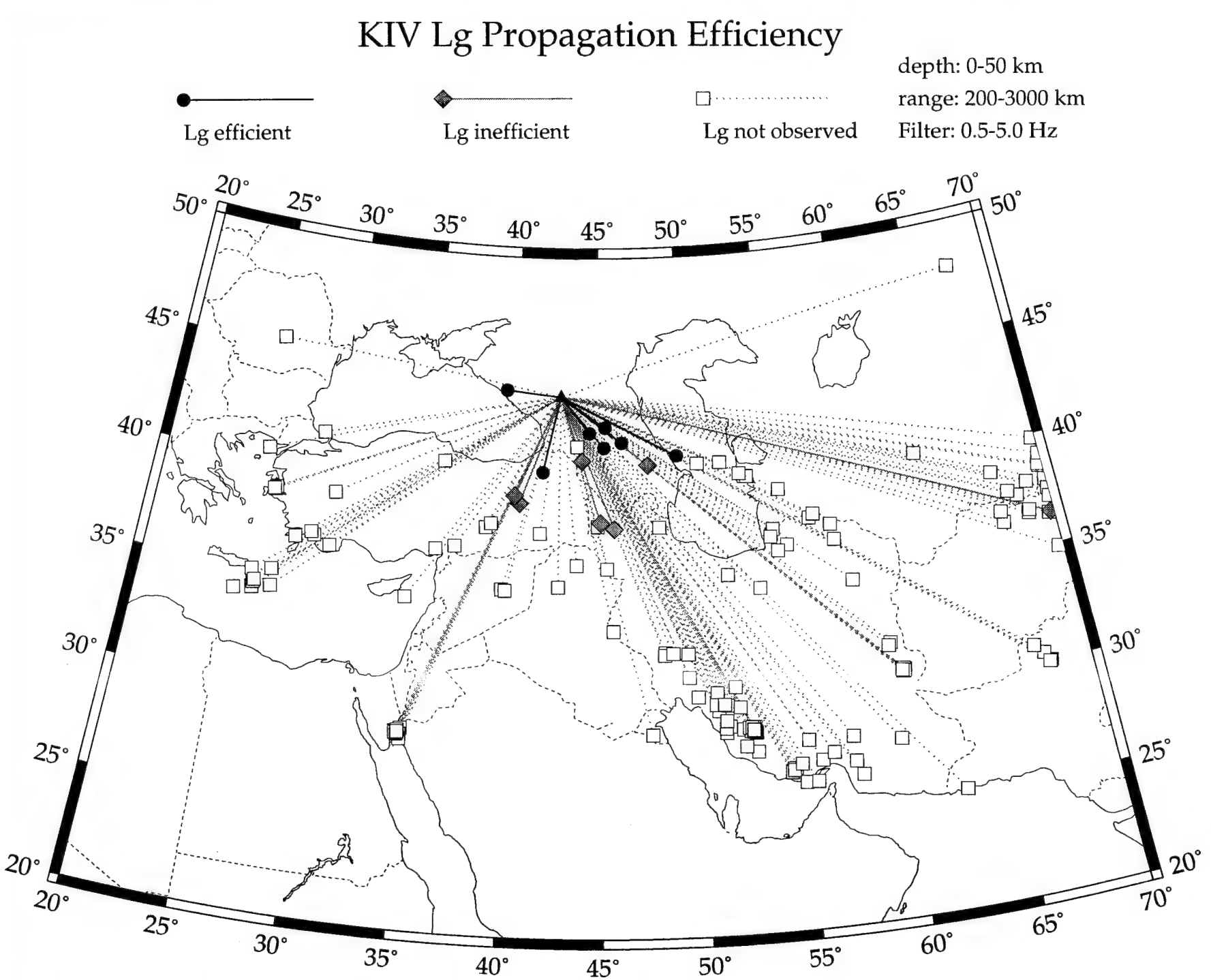

Figure C4: Map showing the efficiency of Lg wave raypaths at station KIV.

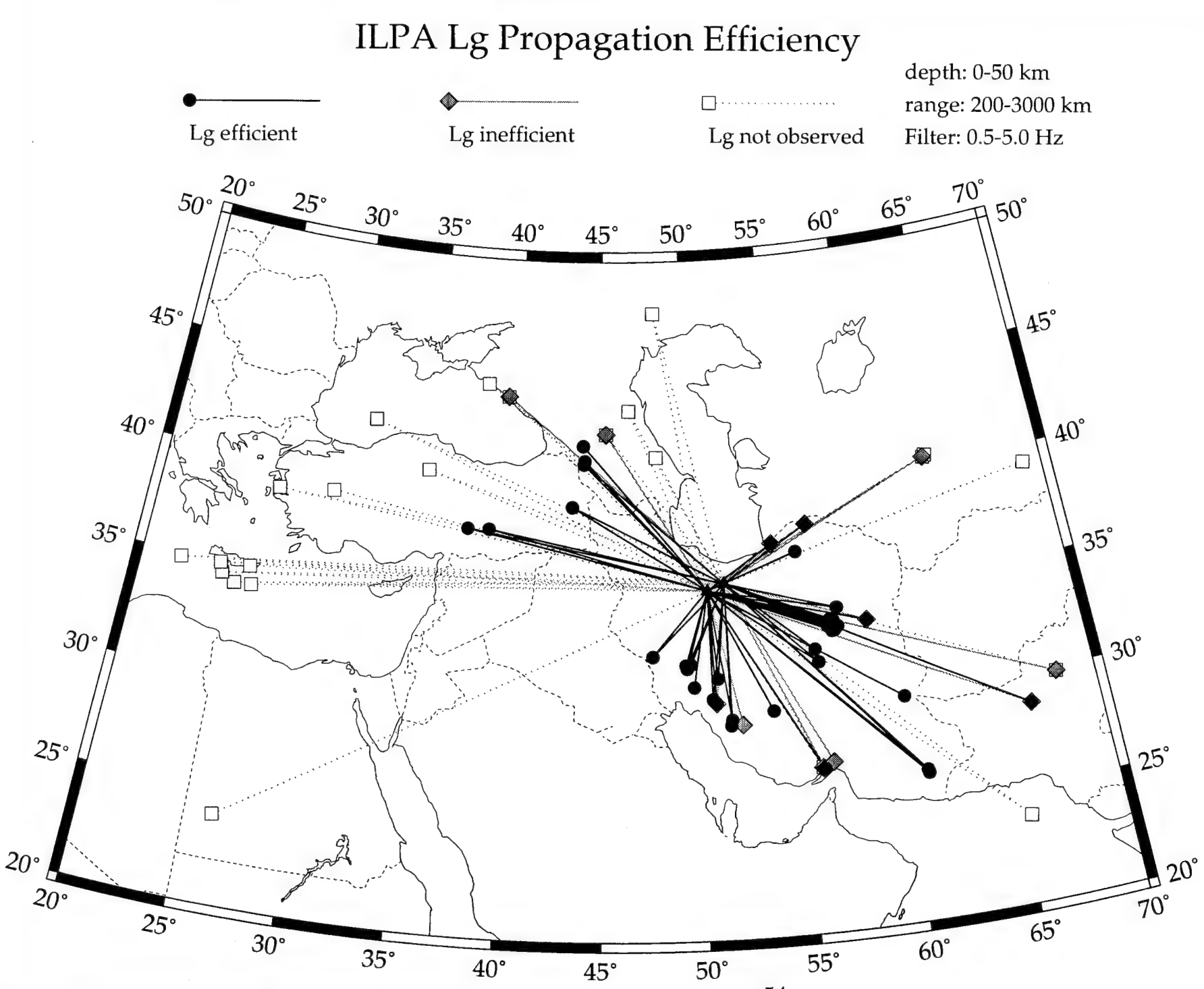

Figure C5: Map showing the efficiency of Lg wave raypaths at ILPA stations.

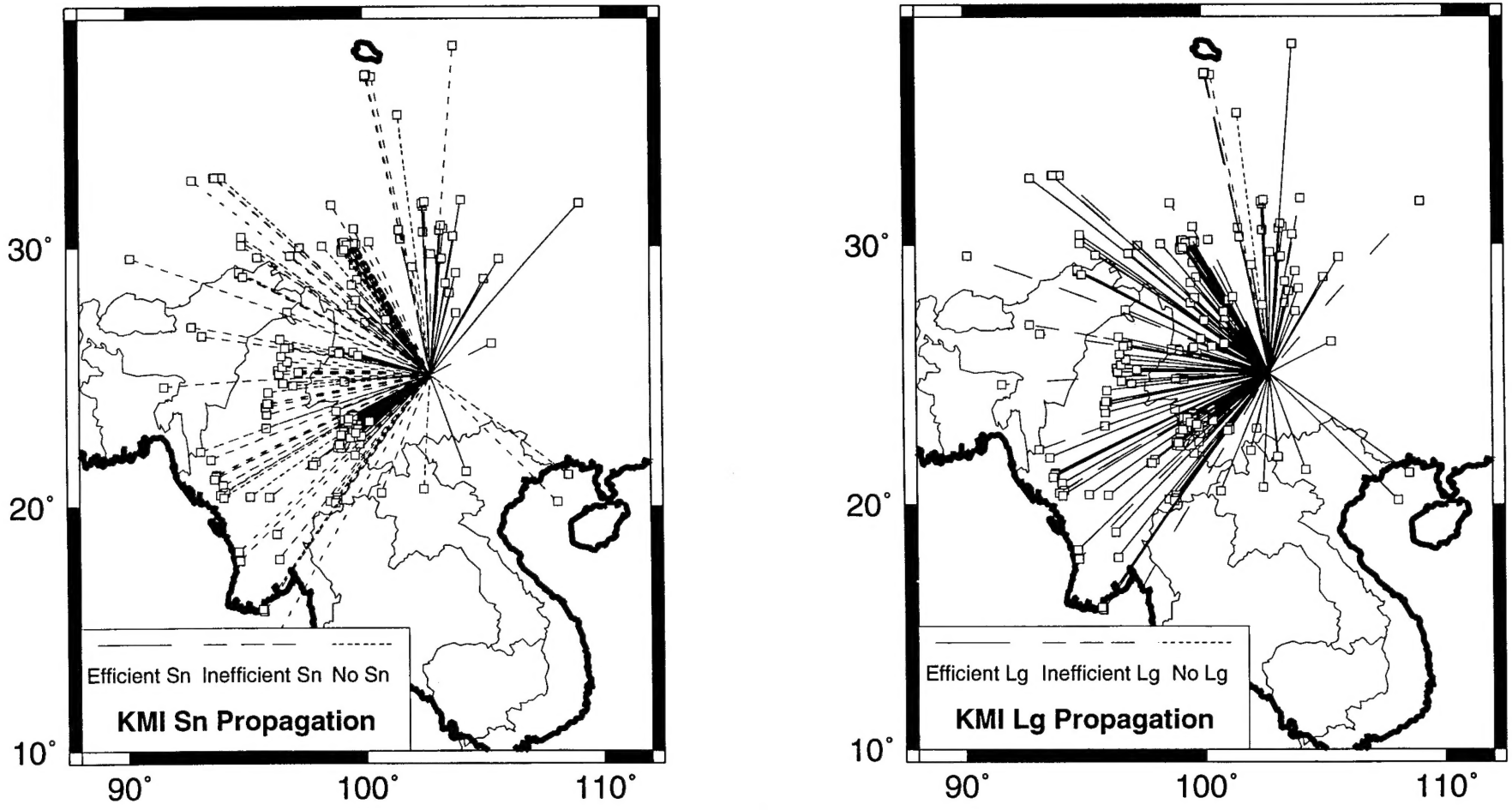

Figure D1: Maps showing propagation efficiency of Sn raypaths (on left) and Lg raypaths (on right) for station KMI.

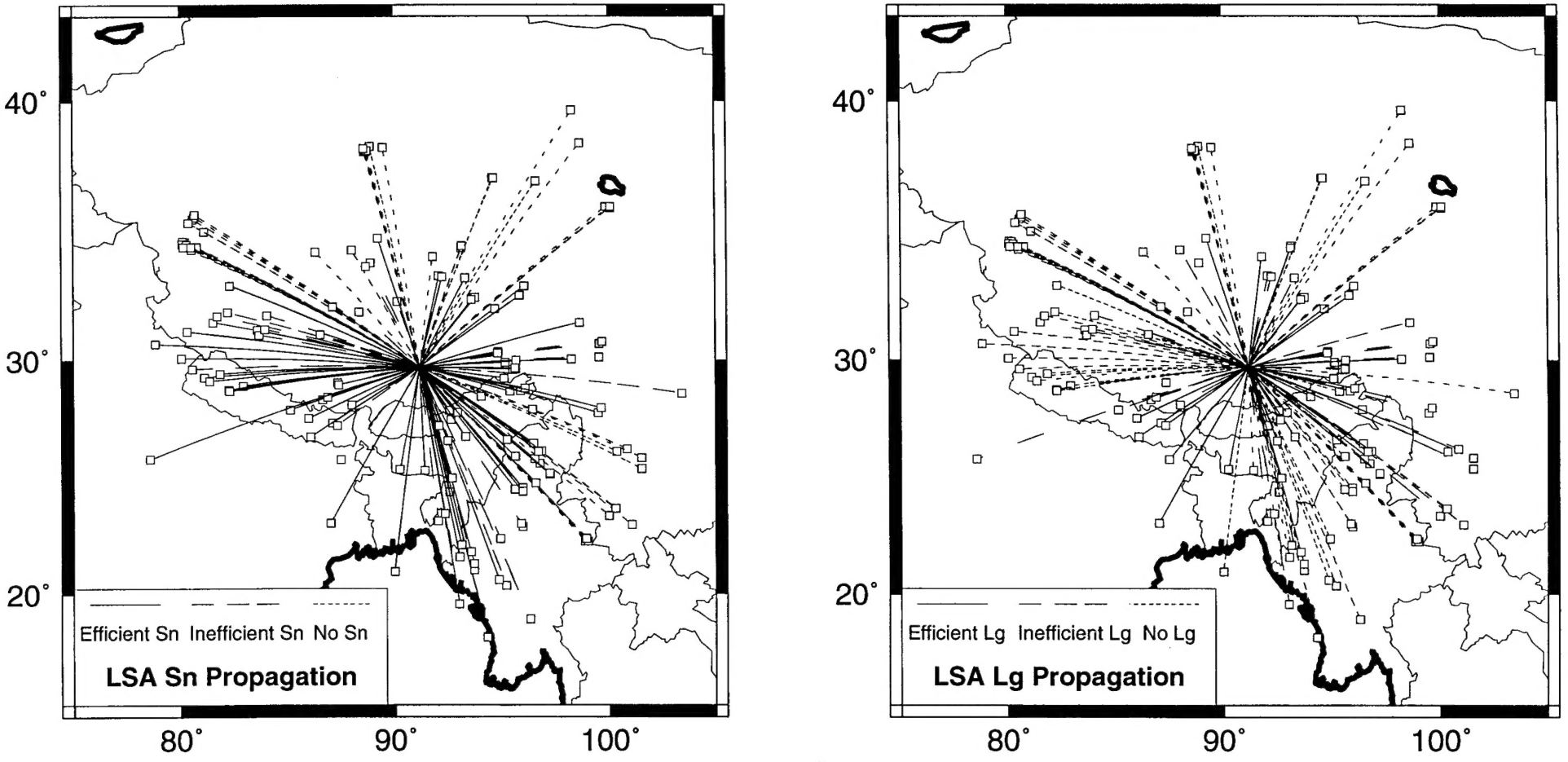

Figure D2: Maps showing propagation efficiency of Sn raypaths (on left) and Lg raypaths (on right) for station LSA.

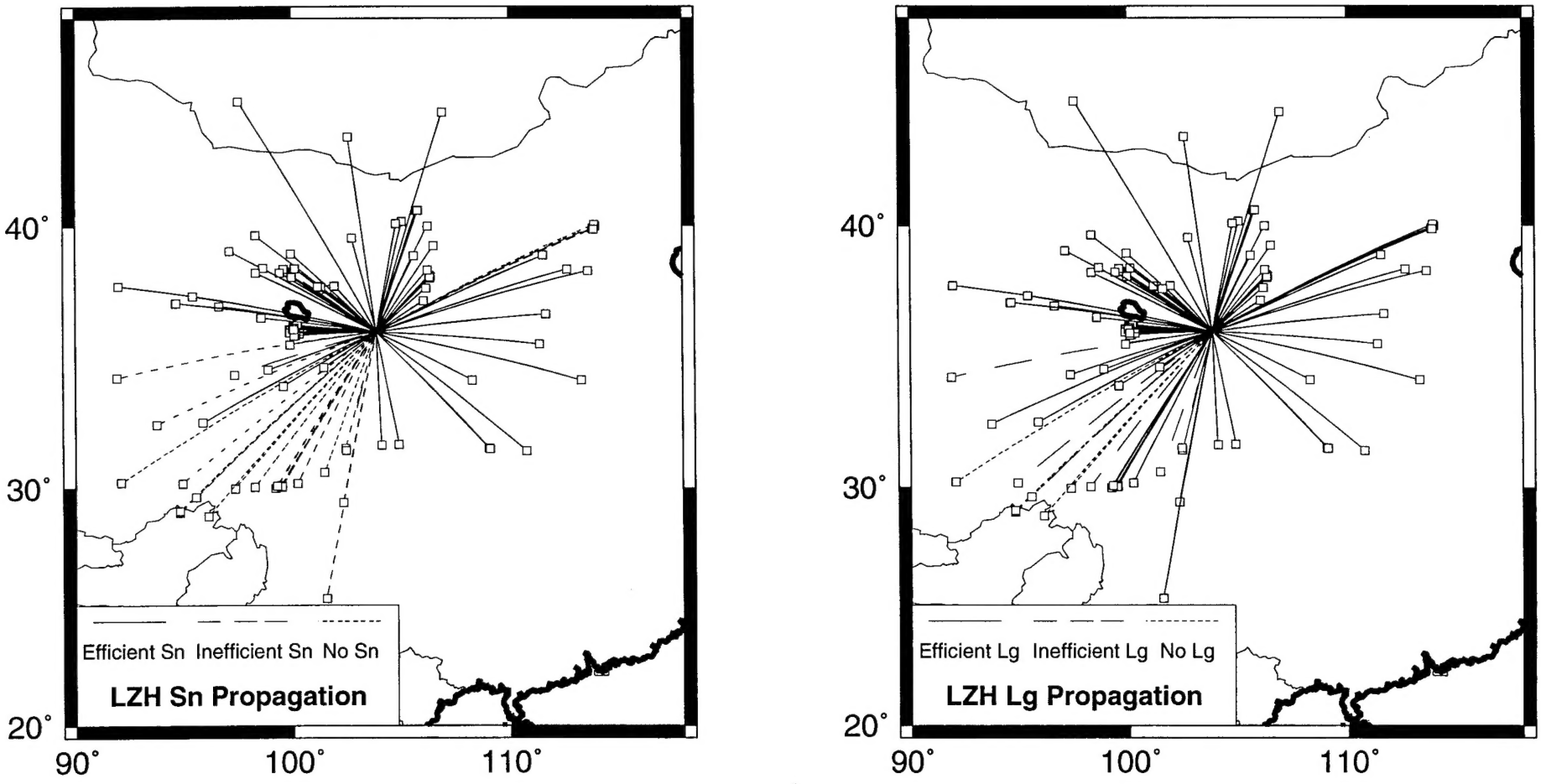

Figure D3: Maps showing propagation efficiency of Sn raypaths (on left) and Lg raypaths (on right) for station LZH.

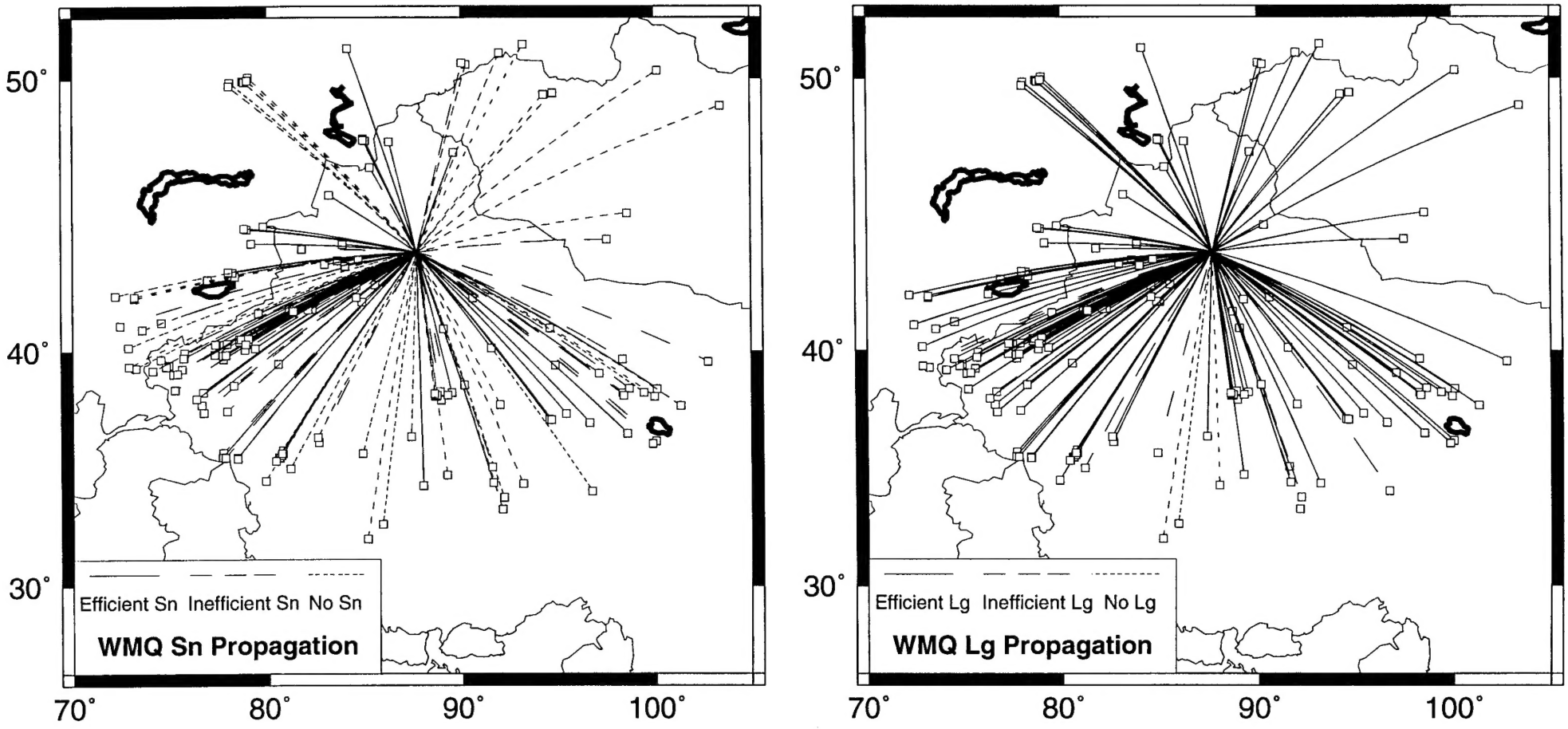

Figure D4: Maps showing propagation efficiency of Sn raypaths (on left) and Lg raypaths (on right) for station WMQ.